Modeling of pressure-dependent background leakages in water distribution networks

Camille Chambon, Olivier Piller, Iraj Mortazavi

HAL Id: hal-04126049
https://hal.inrae.fr/hal-04126049v1

Submitted on 12 Jun 2023

Highlights

- New models with more physical insights of losses in water distribution networks

- Integrating pressure gradient along pipes leads to more accurate leakage models

- Reference hydraulic grade lines and leakage outflows are computed by discretization

- Other new gradually refined models are compared to the existing and reference ones

- New method and models give better predictions without much computation overhead

Modeling of pressure-dependent background leakages in water distribution networks

Camille Chambon[a,b,*], Olivier Piller[a,c], Iraj Mortazavi[b]

[a]*INRAE, UR ETTIS, Cestas, F-33612, France*
[b]*CNAM, M2N, Paris, F-75003, France*
[c]*School of Civil, Environmental, and Mining Eng., Adelaide, SA 5005, Australia*

Abstract

In last decades, several mathematical models have been proposed to simulate background leakages in water distribution networks (WDNs). Some of these models already consider the dependence of leakages to pressure, but they still neglect the gradient of pressure along the pipes. In this article, new models to take into account of this gradient are presented. One of them computes reference background leakage outflows, using a recursive algorithm which discretizes the pipes into sub-pipes until the hydraulic grade line (HGL) along each pipe converges. The other new models consist in gradually refining a state of the art one. All models are then tested and compared on both a single leaky pipe and a WDN derived from a real leaky network. The results of this comparison show clearly the better estimations obtained from our new models when compared to the existing one. Finally, accurate leakage models are essential to estimate the level of leakages and, more generally, the good working order of WDNs. Thus, our new models will help in taking the best decisions for optimal functioning and rehabilitation of the WDNs. Moreover, our recursive discretization approach could be reused for other applications in WDNs, or derived to more general fields of applied mathematics and scientific computation.

Keywords:
water distribution network (WDN), background leakage, pressure-dependent model (PDM), recursive discretization method

1. Introduction

1.1. Water distribution networks

In developed countries, drinkable water is provided to consumers through large interconnected and pressurized water distribution networks (WDNs), composed of pipes, water storage (tanks, reservoirs) and hydraulic equipments (valves, pumps) (fig. 1).
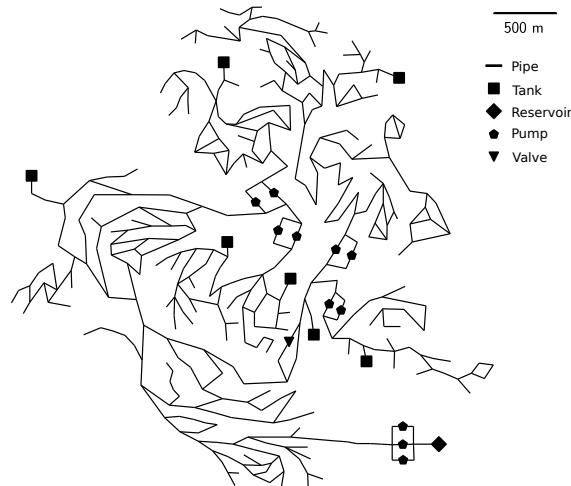
Figure 1: Water distribution network C-Town from [21], composed of 432 pipes, 7 tanks, 1 reservoir, 1 valve and 11 pumps.

Hydraulic models are used to design and operate the WDNs, in order to satisfy the demands of the consumers while limiting the construction and functioning costs. These models are also very helpful to define sampling plans, and to

---

*Corresponding author.
Email address:* `camille.chambon@inrae.fr` (Camille Chambon)

analyze the sensitivity of parameters. Once they are calibrated, WDN models can be coupled to transport models, to optimize the position of new sensors (of pressure, contaminants, etc.), or to measure the benefit of the current ones. Finally, performance and criticality indicators can be calculated to estimate the resilience of the WDNs and their state of degradation [23, 33].

In WDN models, the networks are described by directed graphs, in which the pipes and the equipments are the arcs (a.k.a. links), and the water storage and the junctions connecting the pipes are the vertices (a.k.a. nodes). The incidence matrices associated to the graphs show the relationships between the vertices and the arcs. In steady-state analysis, the heads at water storage nodes are fixed, and the flow rates and the piezometric heads (called just "heads" thereafter) at junctions are computed by solving the mass and energy conservation equations, corresponding respectively to Kirchhoff's first and second laws [3]. Because WDNs are systems which are dynamic, sparse, non-linear, looped, possibly very large and subject to numerous constraints, modeling them has always been a challenge for applied mathematicians and computer scientists, from early [4, 14, 30] to recent [1, 7, 9].

1.2. Background leakages

Leakages appear in WDNs when they age, causing significant water losses. Among the leakages, some are too small to be detected by traditional acoustic equipments; they are called "background leakages", or "diffuse outflows". Even if they are small, background leakages run continuously, often for a long time, and thus contribute greatly to water losses [17]. Because drinkable water is a limited resource which has to be preserved as much as possible, civil engineers and scientists work, since several decades, on detecting and reducing leakages. To do so, they always need for more accurate mathematical models and efficient simulation tools [26].

Currently, one of the best ways to detect leakages in a WDN is to use a dual modeling approach, which consists in transforming the tenuous variations of pressures induced by the leakages to equivalent but clearer flow rate variations [29]. Once the leakages are located, operators can then repair or replace the concerned components. However, further work is needed to determine the conditions of applicability of the dual model to real networks.

Background leakages cannot, by definition, be precisely located. Thus, the only way to reduce them, while preserving a good quality of service, is through a smart control of the pressures [5, 16]. Indeed, since leakages increase much with pressure, the pressures in the WDNs must be sufficient to transport the water from storage to consumers, but low enough to limit the leakages [17].

[11] first proposed a pressure-dependent model (PDM) of the background leakages in water distribution networks, derived from the Torricelli's law, supposing that there is no gradient of pressure along the pipes. Like so, the lineic (i.e., per length unit) leakage outflow in each pipe is independent of the position along the pipe, and is computed from an approximated mean value of the pressure-head into each pipe.

Next, [12] reused the model of [11], combining it with a PDM model of user consumptions based on the Wagner pressure outflow relation (POR) [32]. Thereby, [12] run steady-state simulations of leaky WDNs derived from real networks.

Due to background leakages, the flow rates at the upstream ends of the pipes are different than the ones at their downstream ends. However, in the equations of [12], the computation of the head-loss along each pipe considers a unique value for the flow rate, then neglecting a significant loss of axial momentum along the pipe. Thus, to correct that issue, [10] proposed to add an extra resistance term in the equation of the conservation of energy.

Using a different approach, [15] proposed a slow-transient (a.k.a. unsteady-incompressible, or rigid water column) model to simulate background leakages and inertia phenomena in WDNs subject to slow variations of flows and heads. There, conversely to [10], the friction head-losses are computed by integrating the variation of the flow rates due to background leakages. But, as [10], leakages are simplified to be independent of the pressure in pipes.

All previous models of background leakages have their own advantages and drawbacks. Indeed, the models from [10] and [15] both consider the variations of the flow rates along the pipes, but they neglect the dependence of leakages to pressure. The model of [12] simulates leakages which depend on the pressure, but it neglects the variation of the flow rate along each pipe.

The model from [12] has already been tested by [13], and calibrated by [2, 19]. Thus, we choose it as the state of the art one. However, this model supposes leakage outflows which are independent of the gradients of pressure along the pipes, and computes the friction head-losses without integrating the variation of the flow rate along each pipe.

1.3. Hypothesis, objectives and research strategy

We believe that taking into account the gradient of pressure along the pipes permits to model the background leakages in the WDNs more accurately, and that integrating the variation of the flow rates along the pipes prevents from neglecting a significant loss of axial momentum. Thus, our first objective is to propose new steady-state PDM models of background leakages, which consider the gradients of pressure and integrate the variation of the flow rates along the pipes. This way, civil engineers and WDN managers could benefit from more accurate models to simulate WDNs.

Also, like many other authors (e.g., [1, 4, 7, 9, 14, 30]), we think that WDNs modeling needs the use of rigorous numerical methods. Thus, our second objective is to implement our new models in a generic, efficient and easy to diffuse

way, so they could be easily adapted and reused for other applications in WDNs, or even a source of inspiration for more general fields of applied mathematics and scientific computation.

To achieve these two goals, we will first describe the background models at the pipe scale. Then, we will write the equations of equilibrium at the WDN scale, and propose an optimized Newton algorithm to solve them. Next, we will explain how we check and compare the models to each other. Finally, we will present our results and discuss them.

2. Methods

This section first presents, at the pipe scale, the state of art background leakage model from [12] and our new models. Next, it explains how to integrate all models into the equations of equilibrium of the WDNs, and how to solve these equations. Finally, it describes the networks and method we use to check and compare the models between each other.

In absence of other indications, scalar parameters and variables are denoted in italic (e.g., x), vectors in italic bold (e.g., $\boldsymbol{v}$), matrices in italic bold upper-case (e.g., $\boldsymbol{M}$), scalar functions in upright (e.g., f(x)), vector functions in upright bold (e.g., $\mathbf{f}(\boldsymbol{v})$), matrix functions in upright bold upper-case (e.g., $\mathbf{M}(\boldsymbol{v})$), and sets in blackboard style (e.g., $\mathbb{R}$).

Also, all heads, head-losses and pressure-heads are expressed in mH$_2$O (metres water column), which are consistent to m. All flow rates and leakage outflows are expressed in $1\,\mathrm{s}^{-1}$, rather than $\mathrm{m}^3\,\mathrm{s}^{-1}$, to avoid problems of stability due to machine precision, which could appear when some flow rates are very close to 0 [25].

2.1. Models of background leakages in a single pipe

This sub-section describes how to model a single pipe presenting background leakages, using an existing solution and proposing new ones.

2.1.1. Lineic background leakage outflow

We consider a leaky pipe of length ℓ (in m), and we denote $x \in [0, \ell]$ the position along it. We denote also p_0 and p_ℓ the pressure-heads respectively at $x = 0$ and $x = \ell$. Then, assuming that p_0 and p_ℓ are known, [11] computes the approximated mean pressure in the pipe as

$$\widetilde{p} = \frac{p_0 + p_\ell}{2}. \tag{1}$$

Next, [11] uses the Torricelli's equation to model lineic background leakage outflow (in $1\,\mathrm{s}^{-1}\,\mathrm{m}^{-1}$) along the pipe as

$$\mathrm{q_{LL}}(p) = \beta \left(\left[\widetilde{p} \right]^+ \right)^\alpha, \tag{2}$$

where α corresponds to the type of leakage (unit-less), β represents the level of degradation of the pipe (in $1\,\mathrm{s}^{-1}\,\mathrm{m}^{-1-\alpha}$), and $\left[\widetilde{p} \right]^+$ refers to the positive part of $\widetilde{p}$. Equation (2) can be used to model both local and background leakage outflows. For background leakages, $0.5 < \alpha \leq 2.5$ [17, 20], and $10^{-7} \leq \beta \leq 10^{-1}$ [2, 19].

2.1.2. Theoretical model of background leakage, flow rate and friction head-loss

We suppose here that a function permitting to compute the exact pressure-head at any position $x \in [0, \ell]$ is perfectly known, and we denote it $\mathrm{p^{theo}}(x)$. Then, we can extend eq. (2) to

$$\mathrm{q_{LL}^{theo}}(x) = \beta \left(\left[\mathrm{p^{theo}}(x) \right]^+ \right)^\alpha. \tag{3}$$

Next, we suppose that the flow rate at the middle of the pipe, denoted $q_{0.5}$, is known too. Then, using eq. (3), we can compute the flow rate at any $x \in [0, \ell]$ as:

$$\mathrm{q^{theo}}(x) = q_{0.5} - \int_{\ell/2}^{x} \mathrm{q_{LL}^{theo}}(y)\,\mathrm{d}y. \tag{4}$$

Note: denoting q_0 and q_ℓ the flow rates at respectively $x = 0$ and $x = \ell$, and supposing that either q_0 or q_ℓ is known, then we could have defined $\mathrm{q^{theo}}(x)$ as a function of q_0 or q_ℓ rather than a function of $q_{0.5}$. But the use of $q_{0.5}$ leads to symmetrical and more generic formulation of $\mathrm{q^{theo}}(x)$. We therefore choose to define $\mathrm{q^{theo}}(x)$ as a function of $q_{0.5}$, as in eq. (4).

Finally, we use the Hazen-Williams model [34] to compute the friction head-loss along the pipe. To do so, denoting $\varnothing$ the diameter of the pipe (in mm) and C_{HW} its roughness coefficient (unit-less), and supposing the pipe is cylindrical, we first compute the friction coefficient of the pipe as:

$$f = \frac{10.67}{(1000\,C_{HW})^\gamma\,(\varnothing/1000)^{4.87}}. \tag{5}$$

3

Next, from eq. (4) and eq. (5), we compute the friction head-loss from position 0 to position $x \in [0, \ell]$ as:

$$\xi^{\text{theo}}(x) = f \int_0^x \text{q}^{\text{theo}}(y) \big| \text{q}^{\text{theo}}(y) \big|^{\gamma - 1} \, \mathrm{d}y, \tag{6}$$

where $\gamma = 1.852$ is the Hazen-Williams exponent (unit-less).

Unfortunately, no one knows the function $\text{p}^{\text{theo}}(x)$, and so neither the functions $\text{q}_{\text{LL}}^{\text{theo}}(x)$, $\text{q}^{\text{theo}}(x)$ and $\xi^{\text{theo}}(x)$ $\forall x \in [0, \ell]$. Thus, we propose in next sections 2.1.3 and 2.1.4 to approximate the functions $\big\{ \text{q}_{\text{LL}}^{\text{theo}}(x), \text{q}^{\text{theo}}(x), \xi^{\text{theo}}(x) \big\}$ by different mathematical models, supposing that only p_0, p_ℓ and $q_{0.5}$ are known.

2.1.3. State of the art background leakage model

We choose as the state of the art background leakage model the one initially proposed by [12], and already validated by [12, 13]. In this model, denoted hereafter M0, [12] suppose that the lineic leakage outflow and the flow rate are invariant along the pipe.

To construct M0, [12] reused the function (2) from [11]. Thereby, denoting $\widetilde{q_{LL}} = \beta \big([\widetilde{p}]^+ \big)^\alpha$, [12] computed, at any $x \in [0, \ell]$, the lineic leakage outflow as

$$\text{q}_{\text{LL}}^{\text{M0}}(x) = \widetilde{q_{LL}} \tag{7}$$

and the flow rate as

$$\text{q}^{\text{M0}}(x) = q_{0.5}. \tag{8}$$

Finally, [12] used the Hazen-Williams model [34] to compute the friction head-loss from position 0 to position $x \in [0, \ell]$ as

$$\xi^{\text{M0}}(x) = f \int_0^x q_{0.5} \big| q_{0.5} \big|^{\gamma - 1} \, \mathrm{d}y = f \, q_{0.5} \, \big| q_{0.5} \big|^{\gamma - 1} x. \tag{9}$$

2.1.4. Reference model from recursive discretization

We propose here a new model based on the recursive discretization of a pipe into sub-pipes, until the difference between the hydraulic grade lines (HGLs) along the pipe computed at two consecutive iterations becomes small enough. In this new model, the background leakage outflow rates, the flow rates and the friction head-losses in the initial undiscretized pipe and in each discretized sub-pipe are computed with the functions of the model M0 (see section 2.1.3). Each iteration of the discretization algorithm corresponds to a level of discretization of the pipe.

The functions (7) and (8) are piecewise constant per sub-pipe. They lead to a good numerical approximation of the continuous theoretical functions (3) and (4) providing that the pipe is discretized in enough sub-pipes. Since ξ^{M0} depends linearly on q^{M0}, using ξ^{M0} in each sub-pipe permits to approximate the continuous theoretical function ξ^{theo} as well. Thus, we will consider hereafter this new model as the reference one, and denote it "Ref".

We will now describe the discretization algorithm through a simple example, iteration by iteration. To do so, we first denote q_x, p_x and h_x respectively the flow rate, the pressure-head and the head at the position x along the pipe, $\forall x \in [0, \ell]$. Also, $\forall \{x_1, x_2\} \in [0, \ell] \times [0, \ell]$, $x_1 \leq x_2$, we denote:

$$\widetilde{p_{x_1 x_2}} = \frac{p_{x_1} + p_{x_2}}{2}$$

and

$$\widetilde{q_{LL x_1 x_2}} = \beta \big([\widetilde{p_{x_1 x_2}}]^+ \big)^\alpha$$

respectively the approximated mean pressure-head and the approximated lineic background leakage outflow rate in the interval $[x_1, x_2]$. Finally, we define:

$$q_{L[x_1, x_2]} = \widetilde{q_{LL x_1 x_2}} \, (x_2 - x_1)$$

and

$$\xi_{[x_1, x_2]} = \xi^{\text{M0}}(x_2) - \xi^{\text{M0}}(x_1)$$

respectively the background leakage outflow rate and the friction head-loss cumulated from x_1 to x_2. We explain in next paragraphs what is done at each iteration of the discretization algorithm, following the example on fig. 2.

At iteration 0 (i.e., initial state), the conservation of energy and mass along the undiscretized pipe leads to the system of equations:

$$\begin{pmatrix} h_0^{(0)} - h_\ell^{(0)} - \xi_{[0, \ell]}^{(0)} \\ q_0^{(0)} - q_\ell^{(0)} - q_{L[0, \ell]}^{(0)} \end{pmatrix} = \boldsymbol{0}. \tag{10}$$

Then, the discretization algorithm solves the system (10) to compute the HGL $\boldsymbol{h}^{(0)} = \big(h_0^{(0)}, h_\ell^{(0)} \big)^T$ at positions $\boldsymbol{x}^{(0)} = \big(0, \ell \big)^T$, and goes to iteration 1.
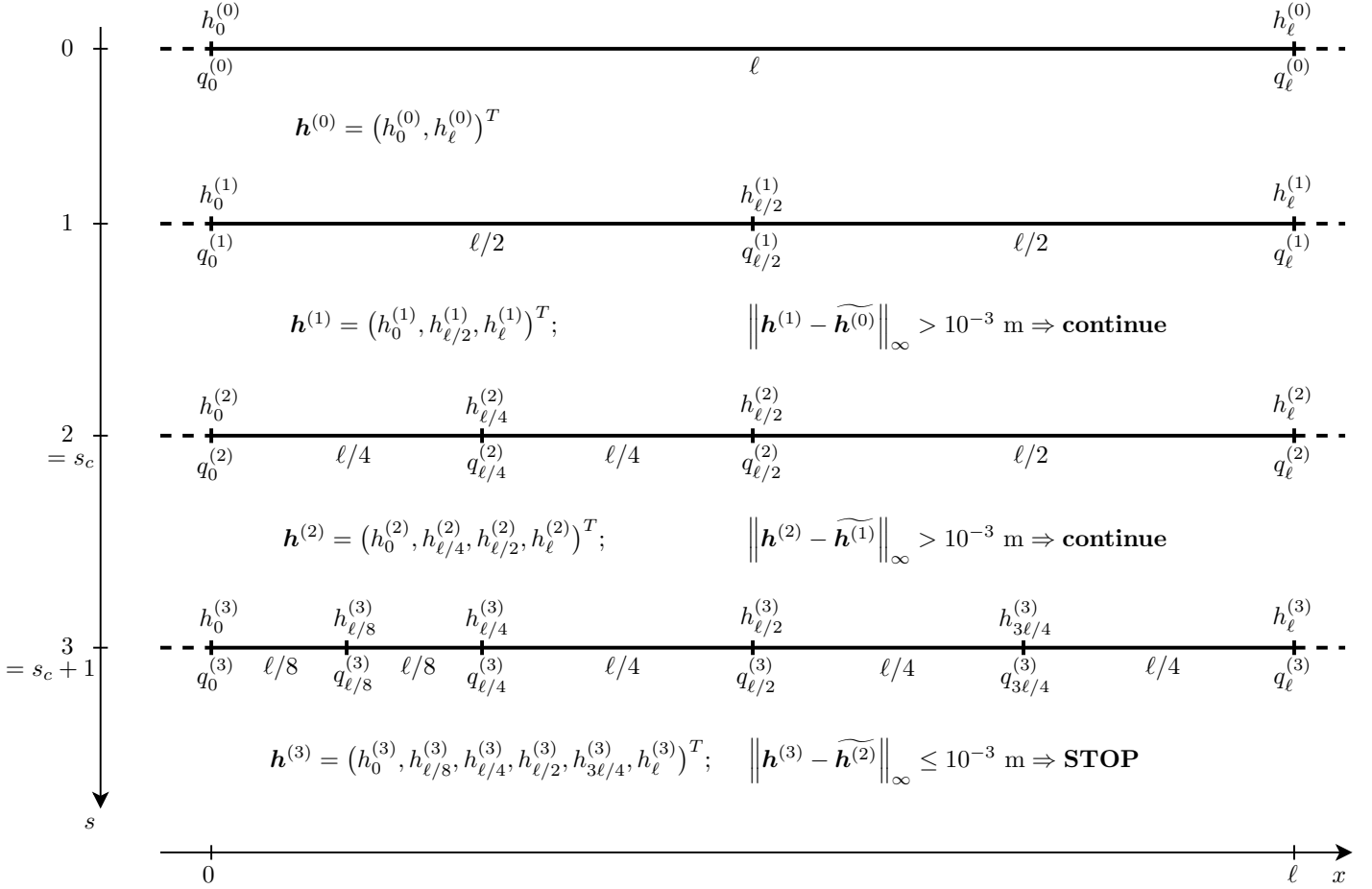
4

Figure 2: Illustration to describe the functioning of the discretization algorithm when applied on a leaky pipe.

At iteration 1, the algorithm discretizes the pipe in 2 sub-pipes of equal length $\ell/2$. Except for their length, the new sub-pipes have exactly the same characteristics as the initial undiscretized pipe: same diameter, roughness, leakage type and level of degradation. The conservation of energy and mass along the sub-pipes leads to the system of equations:

$$
\begin{pmatrix}
h_0^{(1)} - h_{\ell/2}^{(1)} - \xi_{[0,\ell/2]}^{(1)} \\
h_{\ell/2}^{(1)} - h_\ell^{(1)} - \xi_{[\ell/2,\ell]}^{(1)} \\
q_0^{(1)} - q_{\ell/2}^{(1)} - q_{L[0,\ell/2]}^{(1)} \\
q_{\ell/2}^{(1)} - q_\ell^{(1)} - q_{L[\ell/2,\ell]}^{(1)}
\end{pmatrix} = \boldsymbol{0}.
\tag{11}
$$

The discretization algorithm solves the system (11) to compute $\boldsymbol{h}^{(1)} = \left(h_0^{(1)}, h_{\ell/2}^{(1)}, h_\ell^{(1)}\right)^T$ at positions $\boldsymbol{x}^{(1)} = \left(0, \ell/2, \ell\right)^T$. Then, it tests the convergence with the criterion:

$$
\left\|\boldsymbol{h}^{(1)} - \widetilde{\boldsymbol{h}^{(0)}}\right\|_\infty \leq 10^{-3} \, \mathrm{mH_2O},
\tag{12}
$$

where the vector $\widetilde{\boldsymbol{h}^{(0)}}$ contains the values of $\boldsymbol{h}^{(0)}$ interpolated at the positions $\boldsymbol{x}^{(1)}$ using a piecewise cubic Hermite interpolating polynomial (PCHIP), and $10^{-3} \, \mathrm{mH_2O}$ corresponds to $1/10^{\mathrm{th}}$ of the best precision expected when measuring heads physically in a WDN, and so under which the gain in precision becomes negligible. In the example of fig. 2, the criterion (12) is satisfied for the second sub-pipe but not for the first one; then, the algorithm continues to the next iteration.

At iteration 2, the algorithm discretizes only the first sub-pipe (i.e., the sub-pipe where the convergence criterion (12) was not satisfied) in two sub-pipes of equal length $\ell/4$. The conservation of energy and mass along the 3 resulting

sub-pipes leads to:

$$
\begin{pmatrix}
h_0^{(2)} - h_{\ell/4}^{(2)} - \xi_{[0,\ell/4]}^{(2)} \\
h_{\ell/4}^{(2)} - h_{\ell/2}^{(2)} - \xi_{[\ell/4,\ell/2]}^{(2)} \\
h_{\ell/2}^{(2)} - h_{\ell}^{(2)} - \xi_{[\ell/2,\ell]}^{(2)} \\
q_0^{(2)} - q_{\ell/4}^{(2)} - q_{L[0,\ell/4]}^{(2)} \\
q_{\ell/4}^{(2)} - q_{\ell/2}^{(2)} - q_{L[\ell/4,\ell/2]}^{(2)} \\
q_{\ell/2}^{(2)} - q_{\ell}^{(2)} - q_{L[\ell/2,\ell]}^{(2)}
\end{pmatrix}
= \boldsymbol{0}. \tag{13}
$$

The algorithm solves the system (13) to compute $\boldsymbol{h}^{(2)} = (h_0^{(2)}, h_{\ell/4}^{(2)}, h_{\ell/2}^{(2)}, h_{\ell}^{(2)})^T$ at positions $\boldsymbol{x}^{(2)} = (0, \ell/4, \ell/2, \ell)^T$. Then, it tests the convergence as:

$$
\left\| \boldsymbol{h}^{(2)} - \widetilde{\boldsymbol{h}^{(1)}} \right\|_\infty \leq 10^{-3} \, \mathrm{mH_2O}, \tag{14}
$$

where the vector $\widetilde{\boldsymbol{h}^{(1)}}$ contains the values of $\boldsymbol{h}^{(1)}$ interpolated at the positions $\boldsymbol{x}^{(2)}$ using the same method as at iteration 1. The criterion (14) is not satisfied for the first and the third sub-pipes; then, the algorithm continues to the next iteration.

At iteration 3, the algorithm discretizes the first sub-pipe in two sub-pipes of length $\ell/8$, and the third sub-pipe in two sub-pipes of length $\ell/4$. The conservation of energy and mass along the 5 resulting sub-pipes leads to:

$$
\begin{pmatrix}
h_0^{(3)} - h_{\ell/8}^{(3)} - \xi_{[0,\ell/8]}^{(3)} \\
h_{\ell/8}^{(3)} - h_{\ell/4}^{(3)} - \xi_{[\ell/8,\ell/4]}^{(3)} \\
h_{\ell/4}^{(3)} - h_{\ell/2}^{(3)} - \xi_{[\ell/4,\ell/2]}^{(3)} \\
h_{\ell/2}^{(3)} - h_{3\ell/4}^{(3)} - \xi_{[\ell/2,3\ell/4]}^{(3)} \\
h_{3\ell/4}^{(3)} - h_{\ell}^{(3)} - \xi_{[3\ell/4,\ell]}^{(3)} \\
q_0^{(3)} - q_{\ell/8}^{(3)} - q_{L[0,\ell/8]}^{(3)} \\
q_{\ell/8}^{(3)} - q_{\ell/4}^{(3)} - q_{L[\ell/8,\ell/4]}^{(3)} \\
q_{\ell/4}^{(3)} - q_{\ell/2}^{(3)} - q_{L[\ell/4,\ell/2]}^{(3)} \\
q_{\ell/2}^{(3)} - q_{3\ell/4}^{(3)} - q_{L[\ell/2,3\ell/4]}^{(3)} \\
q_{3\ell/4}^{(3)} - q_{\ell}^{(3)} - q_{L[3\ell/4,\ell]}^{(3)}
\end{pmatrix}
= \boldsymbol{0}. \tag{15}
$$

The algorithm solves the system (15) to compute $\boldsymbol{h}^{(3)} = \left(h_0^{(3)}, h_{\ell/8}^{(3)}, h_{\ell/4}^{(3)}, h_{\ell/2}^{(3)}, h_{3\ell/4}^{(3)}, h_{\ell}^{(3)}\right)^T$ at positions $\boldsymbol{x}^{(3)} = \left(0, \ell/8, \ell/4, \ell/2, 3\ell/4, \ell\right)^T$. Then, it tests the convergence with the criterion:

$$
\left\| \boldsymbol{h}^{(1)} - \widetilde{\boldsymbol{h}^{(2)}} \right\|_\infty \leq 10^{-3} \, \mathrm{mH_2O}, \tag{16}
$$

where the vector $\widetilde{\boldsymbol{h}^{(2)}}$ contains the values of $\boldsymbol{h}^{(2)}$ interpolated at the positions $\boldsymbol{x}^{(3)}$ using the same method as at iterations 1 and 2. The criterion (16) is satisfied; then, the algorithm stops. The differences between the HGL computed at iterations 2 and 3 are less than $10^{-3} \, \mathrm{mH_2O}$. Thus, the discretization algorithm converged at iteration $s_c = 2$.

At iteration $s_c + 1 = 3$, we computed the values of h_x and $q_x \; \forall x \in \{0, \ell/8, \ell/4, \ell/2, 3\ell/4, \ell\}$. From each h_x, we can also compute the lineic background leakage outflow rate q_{LLx} as:

$$
q_{LLx} = \beta \left([h_x - u_x]^+ \right)^\alpha, \tag{17}
$$

where u_x is the elevation at the position x along the undiscretized pipe. Finally, from all values of q_{LLx}, q_x and h_x, we can determine by PCHIP interpolation the functions $q_{LL}(x)$, $q(x)$ and $\xi(x)$, $x \in [0, \ell]$. Since these functions compute values that are very close to the ones we would obtain with the theoretical model of section 2.1.2, we will consider them as the reference ones, and denote them $q_{LL}^{Ref}(x)$, $q^{Ref}(x)$ and $\xi^{Ref}(x)$ hereafter.

$\forall x \in [0, \ell]$, the elevation $u_x = u(x)$ at the position x along the undiscretized pipe is computed by linear interpolation from the elevations $u_0 = u(0)$ and $u_\ell = u(\ell)$ at the pipe's extremities, as:

$$
u(x) = \frac{u_\ell - u_0}{\ell} x + u_0. \tag{18}
$$

Actually, graphs of WDNs are generally designed in order to simulate linear pipes. Thus, the linear interpolation of the elevation $u(x)$ is justified supposing that the graph of the network to which belongs the pipe is well-designed, with arcs' slopes not exceeding 3%. However, a more accurate model of elevation could easily replace this linear one, providing that the real elevation of the ground is known at different positions along the pipe.

The convergence criterion, defined at iterations 1, 2 and 3 by respectively eqs. (12), (14) and (16), can be generalized to any iteration $s > 0$ as:

$$\left\| \boldsymbol{h}^{(s-1)} - \widetilde{\boldsymbol{h}^{(s)}} \right\|_\infty \leq 10^{-3}\,\mathrm{mH_2O}, \tag{19}$$

where the vector $\widetilde{\boldsymbol{h}^{(s-1)}}$ contains the PCHIP interpolation of $\boldsymbol{h}^{(s-1)}$ at the positions $\boldsymbol{x}^{(s)}$.

2.1.5. Lineic leakage outflow invariant along the pipe but affine flow rate

We propose here a new model, denoted M1, obtained by refining the state of the art one M0. Indeed, we consider in M1, as for model M0, that the lineic leakage outflow is invariant along the pipe; but we now also suppose, conversely to M0, that for M1 the flow rate is affine along the pipe, as initially proposed by [15].

To do so, denoting $q_{LL}^{\mathrm{M1}} = \mathrm{q}_{LL}^{\mathrm{M1}}(x) = \widetilde{q_{LL}}$, we compute the flow rate at any $x \in [0, \ell]$ as

$$\mathrm{q}^{\mathrm{M1}}(x) = q_{0.5} - q_{LL}^{\mathrm{M1}}\left(x - \frac{\ell}{2}\right). \tag{20}$$

Then, denoting $q_0^{\mathrm{M1}} = \mathrm{q}^{\mathrm{M1}}(0)$, we compute the friction head-loss from position 0 to position $x \in [0, \ell]$ as

$$\xi^{\mathrm{M1}}(x) = \begin{cases} \dfrac{f}{(\gamma+1)\,q_{LL}^{\mathrm{M1}}}\left(\left|q_0^{\mathrm{M1}}\right|^{(\gamma+1)} - \left|\mathrm{q}^{\mathrm{M1}}(x)\right|^{(\gamma+1)}\right) & \text{if } q_{LL}^{\mathrm{M1}} \neq 0 \\ eq.\ (9) & \text{otherwise.} \end{cases} \tag{21}$$

2.1.6. Affine lineic leakage outflow

The next new model, denoted M2, is a refining of model M1. Indeed, in M2, we now consider that the lineic leakage outflow is affine along the pipe. M2 is the first background leakage model which takes into account the gradient of pressure along the pipe without discretization.

To define M2, we first denote $q_{LL0} = \beta\left(\left[p_0\right]^+\right)^\alpha$ and $q_{LL\ell} = \beta\left(\left[p_\ell\right]^+\right)^\alpha$, and we suppose that $\mathrm{q}_{LL}^{\mathrm{M2}}(0) = q_{LL0}$ and $\mathrm{q}_{LL}^{\mathrm{M2}}(\ell) = q_{LL\ell}$. Then, we compute the lineic leakage outflow at any $x \in [0, \ell]$ by linear interpolation as

$$\mathrm{q}_{LL}^{\mathrm{M2}}(x) = \frac{q_{LL\ell} - q_{LL0}}{\ell}\,x + q_{LL0}. \tag{22}$$

Subsequently, denoting $\widehat{\mathrm{x}}(x) = (x + \ell/2)/2$ and $\widehat{\mathrm{q}_{LL}^{\mathrm{M2}}}(x) = \mathrm{q}_{LL}^{\mathrm{M2}} \circ \widehat{\mathrm{x}}(x)$, we compute the flow rate at any $x \in [0, \ell]$ as

$$\mathrm{q}^{\mathrm{M2}}(x) = q_{0.5} - \widehat{\mathrm{q}_{LL}^{\mathrm{M2}}}(x)\left(x - \frac{\ell}{2}\right). \tag{23}$$

Finally, we compute the friction head-loss from position 0 to position $x \in [0, \ell]$ using a Newton-Cotes formula of degree 2, as

$$\xi^{\mathrm{M2}}(x) = f\frac{x}{6}\left(\varphi^{\mathrm{M2}}(0) + 4\,\varphi^{\mathrm{M2}}(x/2) + \varphi^{\mathrm{M2}}(x)\right), \tag{24}$$

where $\varphi^{\mathrm{M2}}(y)$ is the unitary friction head-loss function, defined, $\forall y \in [0, \ell]$, as

$$\varphi^{\mathrm{M2}}(y) = f\mathrm{q}^{\mathrm{M2}}(y)\left|\mathrm{q}^{\mathrm{M2}}(y)\right|^{\gamma-1}. \tag{25}$$

<u>Note</u>: A Newton-Cotes formula of degree 2 allows the exact integration of polynomials of degree 3. Thus, it is accurate enough to model the slope (i.e., 1st derivative estimate) and curvature (i.e., 2nd derivative estimate) of the friction head-loss function.

2.1.7. Pseudo-quadratic lineic leakage outflow

Finally, the last new model that we propose, and denote M3, is a refining of model M2. Indeed, in M3, we consider, as in M2, that the lineic leakage outflow depends on $q_{LL0} = \beta\left(\left[p_0\right]^+\right)^\alpha$ and $q_{LL\ell} = \beta\left(\left[p_\ell\right]^+\right)^\alpha$; but, conversely to M2, M3 now also depends on $\widetilde{q_{LL}} = \beta\left(\left[(p_0 + p_\ell)/2\right]^+\right)^\alpha$. Like so, model M3 takes into account of the gradient of pressure along the pipe, using the three values of lineic leakage outflows q_{LL0}, $q_{LL\ell}$ and $\widetilde{q_{LL}}$.

To define M3, we first suppose that $q_{LL}^{M3}(0) = q_{LL0}$, $q_{LL}^{M3}(\ell/2) = \widetilde{q_{LL}}$ and $q_{LL}^{M3}(\ell) = q_{LL\ell}$, and that $q_{LL}^{M3}(x)$ is a quadratic polynomial $\forall x \in [0, \ell]$. Then, after identification of the coefficients of the polynomial, we obtain:

$$q_{LL}^{M3}(x) = \frac{2\left(q_{LL0} - 2\widetilde{q_{LL}} + q_{LL\ell}\right)}{\ell^2} x^2 - \frac{3\,q_{LL0} - 4\widetilde{q_{LL}} + q_{LL\ell}}{\ell} x + q_{LL0}. \tag{26}$$

Next, simply replacing $q_{LL}^{theo}(y)$ by $q_{LL}^{M3}(y)$ in eq. (4), we compute the flow rate at any $x \in [0, \ell]$ as

$$q^{M3}(x) = q_{0.5} + \left(\frac{\ell}{2} - x\right)\left(\frac{2\left(q_{LL0} - 2\widetilde{q_{LL}} + q_{LL\ell}\right)}{3\,\ell^2}\left(x^2 + x\frac{\ell}{2} + \frac{\ell^2}{4}\right) - \frac{3\,q_{LL0} - 4\widetilde{q_{LL}} + q_{LL\ell}}{2\,\ell}\left(x + \frac{\ell}{2}\right) + q_{LL0}\right). \tag{27}$$

Finally, using the same method as for model M2, we compute the friction head-loss from position 0 to position $x \in [0, \ell]$ as

$$\xi^{M3}(x) = f\frac{x}{6}\left(\varphi^{M3}(0) + 4\,\varphi^{M3}(x/2) + \varphi^{M3}(x)\right). \tag{28}$$

<u>Note</u>: the use of $\widetilde{q_{LL}}$ to compute $q_{LL}^{M3}(x)$ does not make $q_{LL}^{M3}(x)$ of a full higher degree compared to $q_{LL}^{M2}(x)$. Indeed, all of $\{q_{LL0}, \widetilde{q_{LL}}, q_{LL\ell}\}$ are computed using only the two pressure-heads $\{p_0, p_\ell\}$. Hence the qualifying of pseudo-quadratic for M3.

2.2. Modeling of background leakages at WDN scale

This sub-section extends the modeling of background leakages from a single leaky pipe (section 2.1) to a whole leaky WDN.

2.2.1. Variables and notations

For any leaky WDN, we denote n_p the number of cylindrical and longitudinal pipes of lengths $\boldsymbol{\ell} = \left(\ell_1, .., \ell_{n_p}\right)^T \in \mathbb{R}^{n_p}$, n_j the number of junction nodes at which the heads are unknown, n_t and n_r respectively the number of tank and reservoir nodes at which the heads are known and fixed, $n_f = n_t + n_r$ the total number of source nodes, and $N = n_j + n_f$ the total number of nodes.

Next, we denote $\boldsymbol{q_{0.5}} = \left(q_{0.5,1}, .., q_{0.5,n_p}\right)^T \in \mathbb{R}^{n_p}$, $\boldsymbol{h} = \left(h_1, .., h_{n_j}\right)^T \in \mathbb{R}^{n_j}$, $\boldsymbol{h_t} = \left(h_{t,1}, .., h_{t,n_t}\right)^T \in \mathbb{R}^{n_t}$ and $\boldsymbol{h_r} = \left(h_{r,1}, .., h_{r,n_r}\right)^T \in \mathbb{R}^{n_r}$, respectively the unknown flow rates at the middle of the pipes, the unknown heads at junctions, the known heads at tanks and the known heads at reservoirs, and $\boldsymbol{h_f} = \left(\boldsymbol{h_t^T} \mid \boldsymbol{h_r^T}\right)^T \in \mathbb{R}^{n_f}$ and $\boldsymbol{h_N} = \left(\boldsymbol{h^T} \mid \boldsymbol{h_f^T}\right)^T \in \mathbb{R}^N$ the heads respectively at all source nodes and at all nodes. We denote also $\boldsymbol{p} = \left(p_1, .., p_{n_j}\right)^T \in \mathbb{R}^{n_j}$ and $\boldsymbol{l_t} = \left(l_1, .., l_{n_t}\right)^T \in \mathbb{R}^{n_t}$ respectively the pressure-heads at junctions and the water levels at tanks. Then, writing $\boldsymbol{u} = \left(u_1, .., u_{n_j}\right)^T \in \mathbb{R}^{n_j}$, $\boldsymbol{u_t} = \left(u_1, .., u_{n_t}\right)^T \in \mathbb{R}^{n_t}$ and $\boldsymbol{u_r} = \left(u_1, .., u_{n_r}\right)^T \in \mathbb{R}^{n_r}$ respectively the elevations at junctions, the elevations at tank bottoms (i.e., where water level is zero), and the elevations of water surface in reservoirs, we have the relations:

$$\boldsymbol{p} = \boldsymbol{h} - \boldsymbol{u} \tag{29}$$

at junctions,

$$\boldsymbol{l_t} = \boldsymbol{h_t} - \boldsymbol{u_t} \tag{30}$$

at tanks, and

$$\boldsymbol{h_r} = \boldsymbol{u_r} \tag{31}$$

at reservoirs.

Next, we denote the $n_j \times n_p$ junction-pipe, the $n_t \times n_p$ tank-pipe, and the $n_r \times n_p$ reservoir-pipe incidence matrices as respectively $\boldsymbol{A}$, $\boldsymbol{A_t}$ and $\boldsymbol{A_r}$, the $N \times n_f$ source-pipe incidence matrix as $\boldsymbol{A_f} = \left(\boldsymbol{A_t^T} \mid \boldsymbol{A_r^T}\right)^T$, and the $N \times n_p$ node-pipe incidence matrix as $\boldsymbol{A_N} = \left(\boldsymbol{A^T} \mid \boldsymbol{A_f^T}\right)^T$, and we denote the positive and the negative parts of $\boldsymbol{A}$ as respectively $\boldsymbol{A^+}$ and $\boldsymbol{A^-}$. Also, we denote $\mathbf{q_0}(\boldsymbol{q_{0.5}}, \boldsymbol{h_N})$, $\mathbf{q_\ell}(\boldsymbol{q_{0.5}}, \boldsymbol{h_N})$ and $\boldsymbol{\xi}(\boldsymbol{q_{0.5}}, \boldsymbol{h_N})$, the vector functions of $\mathbb{R}^{n_p \times N}$ to $\mathbb{R}^{n_p}$, defined as $\mathbf{q_0}(\boldsymbol{q_{0.5}}, \boldsymbol{h_N}) = \boldsymbol{q_0}$, $\mathbf{q_\ell}(\boldsymbol{q_{0.5}}, \boldsymbol{h_N}) = \boldsymbol{q_\ell}$ and $\boldsymbol{\xi}(\boldsymbol{q_{0.5}}, \boldsymbol{h_N}) = \boldsymbol{\xi_\ell}$. $\forall k \in \{1..n_p\}$, $q_{0,k} = q_k(0)$, $q_{\ell,k} = q_k(\ell_k)$ and $\xi_{\ell,k} = \xi_k(\ell_k)$ are computed using one of the models $\{M0..M3\}$ described in sections 2.1.3 and 2.1.5 to 2.1.7.

Finally, we denote $\boldsymbol{d} = \left(d_1, .., d_{n_j}\right)^T \in \mathbb{R}^{n_j}$ the demands of consumers at junctions, and p_m and p_s respectively the minimal and the service pressure-heads such that $p_s > p_m$. Then, $\forall i \in \{1..n_j\}$, the scalar function to compute the fraction of pressure-head at junction i is defined as

$$z(p_i) = \frac{p_i - p_m}{p_s - p_m}, \tag{32}$$

and the Wagner scalar function [32] to compute the user consumption at i as

$$c_i(p_i) = \begin{cases} 0 & \text{if } z(p_i) \leq 0 \\ d_i \sqrt{z(p_i)} & \text{if } 0 < z(p_i) < 1 \\ d_i & \text{if } z(p_i) \geq 1. \end{cases} \tag{33}$$

From eqs. (29) and (33), we denote $\mathbf{c}(\boldsymbol{h}) = \left(c_1(h_1), .., c_{n_j}(h_{n_j})\right)^T$ the vector function of $\mathbb{R}^{n_j}$ to $\mathbb{R}^{n_j}$ to compute the user consumptions at all junctions.

2.2.2. Equations of equilibrium

To find the unknown flow rates $\boldsymbol{q_{0.5}}$ and heads $\boldsymbol{h}$ in a WDN at steady-state, we need to solve the non-linear system of equations:

$$\boldsymbol{\rho}(\boldsymbol{q_{0.5}}, \boldsymbol{h}) = \begin{pmatrix} \boldsymbol{\xi}(\boldsymbol{q_{0.5}}, \boldsymbol{h_N}) - \boldsymbol{A}^T \boldsymbol{h} - \boldsymbol{A}_f^T \boldsymbol{h_f} \\ \boldsymbol{A}^- \, \mathbf{q_\ell}(\boldsymbol{q_{0.5}}, \boldsymbol{h_N}) - \boldsymbol{A}^+ \, \mathbf{q_0}(\boldsymbol{q_{0.5}}, \boldsymbol{h_N}) - \mathbf{c}(\boldsymbol{h}) \end{pmatrix} = \boldsymbol{0}, \tag{34}$$

where

$$\boldsymbol{\xi}(\boldsymbol{q_{0.5}}, \boldsymbol{h_N}) - \boldsymbol{A}^T \boldsymbol{h} - \boldsymbol{A}_f^T \boldsymbol{h_f} = \boldsymbol{\rho_e} \tag{35}$$

are the energy residuals in pipes, and

$$\boldsymbol{A}^- \, \mathbf{q_\ell}(\boldsymbol{q_{0.5}}, \boldsymbol{h_N}) - \boldsymbol{A}^+ \, \mathbf{q_0}(\boldsymbol{q_{0.5}}, \boldsymbol{h_N}) - \mathbf{c}(\boldsymbol{h}) = \boldsymbol{\rho_m} \tag{36}$$

the mass residuals at junctions. The use of matrices $\{\boldsymbol{A}^+, \boldsymbol{A}^-\}$ and flow rates $\{\mathbf{q_0}(\boldsymbol{q_{0.5}}, \boldsymbol{h_N}), \mathbf{q_\ell}(\boldsymbol{q_{0.5}}, \boldsymbol{h_N})\}$, needed to ensure the mass conservation at junctions when simulating PDM background leakages, represent a new formulation of the equations of equilibrium.

2.2.3. Newton algorithm

To solve eq. (34), we choose to use the Newton's method. To do so, we first define the Jacobian matrix function of eq. (34) as:

$$\mathbf{J} = \begin{pmatrix} \mathbf{J_{11}} & \mathbf{J_{12}} \\ \mathbf{J_{21}} & \mathbf{J_{22}} \end{pmatrix} \tag{37}$$

where,

$$\mathbf{J_{11}} = \frac{\partial \boldsymbol{\xi}}{\partial \boldsymbol{q_{0.5}}} \quad , \quad \mathbf{J_{12}} = \frac{\partial \boldsymbol{\xi}}{\partial \boldsymbol{h}} - \boldsymbol{A}^T \quad , \quad \mathbf{J_{21}} = -\left(\boldsymbol{A}^+ - \boldsymbol{A}^-\right) = -\boldsymbol{A} \quad \text{and} \quad \mathbf{J_{22}} = \boldsymbol{A}^- \frac{\partial \mathbf{q_\ell}}{\partial \boldsymbol{h}} - \boldsymbol{A}^+ \frac{\partial \mathbf{q_0}}{\partial \boldsymbol{h}} - \frac{\partial \mathbf{c}}{\partial \boldsymbol{h}}. \tag{38}$$

Then, denoting $\boldsymbol{q_{0.5}^{(0)}}$ the initial guesses of flow rates at middle of pipes, $\boldsymbol{h}^{(0)}$ the ones of heads at junctions, and $\boldsymbol{J}^{(m)} = \mathbf{J}(\boldsymbol{q_{0.5}^{(m)}}, \boldsymbol{h}^{(m)})$ the Jacobian matrix of $\boldsymbol{\rho}^{(m)} = \boldsymbol{\rho}(\boldsymbol{q_{0.5}^{(m)}}, \boldsymbol{h}^{(m)})$ at iteration m, and supposing that $\boldsymbol{J}^{(m)}$ is invertible, the Newton algorithm consists in computing, for $m = 0, 1, 2, ...$, the iterates $\boldsymbol{q_{0.5}^{(m+1)}}$ and $\boldsymbol{h}^{(m+1)}$ as

$$\begin{pmatrix} \boldsymbol{q_{0.5}^{(m+1)}} \\ \boldsymbol{h}^{(m+1)} \end{pmatrix} = \begin{pmatrix} \boldsymbol{q_{0.5}^{(m)}} \\ \boldsymbol{h}^{(m)} \end{pmatrix} - \left(\boldsymbol{J}^{(m)}\right)^{-1} \begin{pmatrix} \boldsymbol{\rho_e^{(m)}} \\ \boldsymbol{\rho_m^{(m)}} \end{pmatrix}, \tag{39}$$

until the differences between two successive iterates become less than a given tolerance.

In eq. (39), computing the iterates by inverting the possibly very large matrix $\boldsymbol{J}^{(m)} \in \mathbb{R}^{(n_p+n_j) \times (n_p+n_j)}$ can be very time consuming. Thus, we rather look for the descent directions on $\boldsymbol{q_{0.5}^{(m)}}$ and $\boldsymbol{h}^{(m)}$, defined respectively as

$$\boldsymbol{\delta_{q_{0.5}}^{(m)}} = \boldsymbol{q_{0.5}^{(m+1)}} - \boldsymbol{q_{0.5}^{(m)}} \qquad \text{and} \qquad \boldsymbol{\delta_h^{(m)}} = \boldsymbol{h}^{(m+1)} - \boldsymbol{h}^{(m)}, \tag{40}$$

and which satisfy the linear system:

$$\begin{pmatrix} \mathbf{J_{11}^{(m)}} & \mathbf{J_{12}^{(m)}} \\ \mathbf{J_{21}^{(m)}} & \mathbf{J_{22}^{(m)}} \end{pmatrix} \begin{pmatrix} \boldsymbol{\delta_{q_{0.5}}^{(m)}} \\ \boldsymbol{\delta_h^{(m)}} \end{pmatrix} = - \begin{pmatrix} \boldsymbol{\rho_e^{(m)}} \\ \boldsymbol{\rho_m^{(m)}} \end{pmatrix}, \tag{41}$$

or, in developed form:

$$\begin{pmatrix} \mathbf{J_{11}^{(m)}} \boldsymbol{\delta_{q_{0.5}}^{(m)}} + \mathbf{J_{12}^{(m)}} \boldsymbol{\delta_h^{(m)}} \\ \mathbf{J_{21}^{(m)}} \boldsymbol{\delta_{q_{0.5}}^{(m)}} + \mathbf{J_{22}^{(m)}} \boldsymbol{\delta_h^{(m)}} \end{pmatrix} = - \begin{pmatrix} \boldsymbol{\rho_e^{(m)}} \\ \boldsymbol{\rho_m^{(m)}} \end{pmatrix}. \tag{42}$$

To solve the system (42), we first use its first equation (i.e., row) to express $\boldsymbol{\delta}_{\boldsymbol{q}_{0.5}}^{(m)}$ in function of $\boldsymbol{\delta}_{\boldsymbol{h}}^{(m)}$:

$$\boldsymbol{\delta}_{\boldsymbol{q}_{0.5}}^{(m)} = -\left(\boldsymbol{J}_{11}^{(m)}\right)^{-1}\left(\boldsymbol{J}_{12}^{(m)}\boldsymbol{\delta}_{\boldsymbol{h}}^{(m)} + \boldsymbol{\rho}_{\boldsymbol{e}}^{(m)}\right), \tag{43}$$

assuming that the diagonal matrix $\boldsymbol{J}_{11}^{(m)} \in \mathbb{R}^{n_p \times n_p}$ is invertible. Next, we substitute (43) into the second equation of the system (42) to obtain:

$$\boldsymbol{S}^{(m)}\,\boldsymbol{\delta}_{\boldsymbol{h}}^{(m)} = \boldsymbol{J}_{21}^{(m)}\left(\boldsymbol{J}_{11}^{(m)}\right)^{-1}\boldsymbol{\rho}_{\boldsymbol{e}}^{(m)} - \boldsymbol{\rho}_{\boldsymbol{m}}^{(m)}, \tag{44}$$

where $\boldsymbol{S}^{(m)} \in \mathbb{R}^{n_j \times n_j}$ is the Schur complement of the block $\boldsymbol{J}_{11}^{(m)}$, and is defined as:

$$\boldsymbol{S}^{(m)} = \boldsymbol{J}_{22}^{(m)} - \boldsymbol{J}_{21}^{(m)}\left(\boldsymbol{J}_{11}^{(m)}\right)^{-1}\boldsymbol{J}_{12}^{(m)}. \tag{45}$$

Contrary to the WDN models which do not simulate PDM background leakages, it is not possible here to use a Cholesky factorization to compute $\boldsymbol{\delta}_{\boldsymbol{h}}^{(m)}$ from eq. (44), because $\boldsymbol{S}^{(m)}$ is not symmetric. Thus, since $\boldsymbol{S}^{(m)}$ is highly sparse, the most suitable method to compute $\boldsymbol{\delta}_{\boldsymbol{h}}^{(m)}$ is to use a direct sparse LU factorization, as long as $\boldsymbol{S}^{(m)}$ is invertible. Next, once $\boldsymbol{\delta}_{\boldsymbol{h}}^{(m)}$ is calculated, we can easily compute $\boldsymbol{\delta}_{\boldsymbol{q}_{0.5}}^{(m)}$ from eq. (43) because $\boldsymbol{J}_{11}^{(m)}$ is diagonal and supposed invertible.

Finally, after computing both $\boldsymbol{\delta}_{\boldsymbol{h}}^{(m)}$ and $\boldsymbol{\delta}_{\boldsymbol{q}_{0.5}}^{(m)}$, we can replace

$$-\left(\boldsymbol{J}^{(m)}\right)^{-1}\begin{pmatrix}\boldsymbol{\rho}_{\boldsymbol{e}}^{(m)}\\\boldsymbol{\rho}_{\boldsymbol{m}}^{(m)}\end{pmatrix} \qquad \text{by} \qquad \begin{pmatrix}\boldsymbol{\delta}_{\boldsymbol{q}_{0.5}}^{(m)}\\\boldsymbol{\delta}_{\boldsymbol{h}}^{(m)}\end{pmatrix}$$

in eq. (39), and compute the new iterates $\boldsymbol{q}_{0.5}^{(m+1)}$ and $\boldsymbol{h}^{(m+1)}$ as

$$\begin{pmatrix}\boldsymbol{q}_{0.5}^{(m+1)}\\\boldsymbol{h}^{(m+1)}\end{pmatrix} = \begin{pmatrix}\boldsymbol{q}_{0.5}^{(m)}\\\boldsymbol{h}^{(m)}\end{pmatrix} + \begin{pmatrix}\boldsymbol{\delta}_{\boldsymbol{q}_{0.5}}^{(m)}\\\boldsymbol{\delta}_{\boldsymbol{h}}^{(m)}\end{pmatrix}. \tag{46}$$

To test for the convergence of scheme (46), we use a stop criterion that is almost the same as the one already used by [9]. Indeed, we consider that the convergence is reached as soon as, $\forall \boldsymbol{y} \in \{\boldsymbol{q}_{0.5}, \boldsymbol{h}\}$,

$$\begin{cases}\dfrac{\left\|\boldsymbol{y}^{(m+1)} - \boldsymbol{y}^{(m)}\right\|_\infty}{\left\|\boldsymbol{y}^{(m+1)}\right\|_\infty} \leq 10^{-6} & \text{if } \left\|\boldsymbol{y}^{(m+1)}\right\|_\infty \geq 10^{-6}\\[2mm]\left\|\boldsymbol{y}^{(m+1)} - \boldsymbol{y}^{(m)}\right\|_\infty \leq 10^{-6} & \text{otherwise.}\end{cases} \tag{47}$$

The only difference with [9] is that our version of the criterion also handles the case where $\left\|\boldsymbol{y}^{(m+1)} - \boldsymbol{y}^{(m)}\right\|_\infty \leq 10^{-6}$.

2.3. Extension of the discretization algorithm to WDN scale

At section 2.1.4, we proposed a new reference model "Ref", based on the recursive discretization of a pipe into sub-pipes until the difference between the hydraulic grade lines (HGLs) of two consecutive discretization levels becomes small enough.

To extend the algorithm to the scale of a whole WDN, we simply apply, at each iteration $s > 0$ of the discretization algorithm ($s = 0$ corresponds to the solving of the undiscretized network), the following procedure:

1. iterate over each pipe $k \in \{1..n_p\}$ of the WDN, to look if k needs, according to the convergence criterion (19), to be discretized more,
2. for each (sub-)pipe that needs to be (re-)discretized: replace the (sub-)pipe by 2 (sub-)sub-pipes connected by a new intermediate junction node,
3. and solve the system of energy and mass conservation equations (34) that describes the new discretized WDN, for the flow rates and heads at the extremity nodes of the pipes and the interior points of the discretized pipe at the same time,

until the convergence criterion (19) becomes satisfied $\forall k \in \{1..n_p\}$. Then, at the last iteration, the heads computed at the extremities of the undiscretized pipes are the reference heads. Also, in each pipe k, the flow rates along k obtained at the last iteration permit to compute, by PCHIP interpolation, the reference flow rate at the middle of k.

In the 2$^{\text{nd}}$ item of the procedure above, the new intermediate junction nodes have no demand, and their elevations are computed by linear interpolation from the elevations at the extremities of the (sub-)pipes. For the same reasons as the ones already exposed at a pipe's scale (see section 2.1.4), using linear interpolation to compute the elevations of the intermediate junction nodes is justified.

10

In the 3$^{\text{rd}}$ item of the procedure, the system of equations that models the new discretized WDN is composed of all the sub-systems of equations that describe the discretized and undiscretized pipes. E.g., for any discretized pipe, this sub-system can be one of eqs. (11), (13) and (15).

2.4. Numerical enhancements

Some sources of instabilities could hinder the convergence of the Newton algorithm described in section 2.2.3. We present them below, along with numerical enhancements to overcome them.

All these numerical enhancements are of primary importance to ensure the convergence of the Newton algorithm in many common situations. However, we choose, to preserve readability and remain focus on background leakage modeling, to describe them in the supplementary material.

2.4.1. Pipes with zero flows

To compute $\left(\boldsymbol{J}_{11}^{(m)} \right)^{-1}$ and solve the system eq. (41) with models M0 and Ref, we need, for each (sub-)pipe k, to inverse the derivative of the friction head-loss function (9) for $x = \ell_k$ with respect to $q_{0.5,k}$. This derivative is defined as

$$\frac{\mathrm{d}\xi_k^{\text{M0}}(\ell_k)}{\mathrm{d}q_{0.5,k}}(q_{0.5,k}) = \gamma\, f_k\, \ell_k\, \left| q_{0.5,k} \right|^{\gamma-1}. \tag{48}$$

However, eq. (48) gives 0 when $q_{0.5,k} = 0$. Thus, using eq. (48) as it may lead to division by zero errors.

To avoid these errors, we choose to reuse the cubic regularization of eq. (9) and the quadratic regularization of eq. (48) initially proposed by [22].

2.4.2. Consumer nodes with pressure-heads close to minimum or service pressure-head

For each model, we need to compute at each (intermediate-)junction node i the derivative of the fraction of pressure-head z_i (eq. (32)) with respect to the pressure-head $p_i = h_i - u_i$, as

$$\frac{\mathrm{d}z_i}{\mathrm{d}p_i} = \frac{1}{p_s - p_m}, \tag{49}$$

and next the derivative of the Wagner user consumption c_i (eq. (33)) with respect to p_i, as

$$\frac{\mathrm{d}c_i}{\mathrm{d}p_i}(p_i) = \begin{cases} d_i \dfrac{\mathrm{d}z_i}{\mathrm{d}p_i} \dfrac{1}{2\sqrt{z_i(p_i)}} & \text{if } 0 < z_i(p_i) < 1 \\ 0 & \text{otherwise.} \end{cases} \tag{50}$$

However, eq. (50) is undefined at $p_i = p_m$ and discontinuous at $p_i = p_s$. Thus, using eq. (50) as it may lead to convergence errors when p_i is close to p_m or p_s.

To avoid these errors, we choose to reuse the cubic regularizations of eq. (33) and the quadratic regularizations of eq. (50) initially proposed by [24].

2.4.3. Leaky pipe(s) with pressure(s) close to zero

For each leaky pipe k, we need to compute the derivative with respect to p_k of the function

$$q_{\text{LL,k}}(p_k) = \beta_k \left(\left[p_k \right]^+ \right)^{\alpha_k}, \tag{51}$$

for one, several or all of $p_k \in \{p_{0,k}, \widetilde{p_k}, p_{\ell,k}\}$, according to the background leakage model we use (i.e., M0/Ref, M1, M2 or M3). The derivative of eq. (51) is defined as:

$$\frac{\mathrm{d}q_{\text{LL,k}}}{\mathrm{d}p_k}(p_k) = \begin{cases} \alpha_k\, \beta_k\, p_k^{\alpha_k-1} & \text{if } p_k > 0 \\ 0 & \text{otherwise.} \end{cases} \tag{52}$$

However, eq. (52) is discontinuous at $p_k = 0 \; \forall \alpha_k \in\,]0.5, 1[$. Thus, using eq. (52) as it could lead to convergence errors when p_k is close to 0 and $\alpha_k \in\,]0.5, 1]$.

To avoid these errors, we implement our own new cubic regularization of eq. (51) and quadratic regularization of eq. (52) for pressure-heads close to 0. These regularizations are described in the supplementary material.
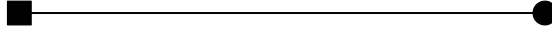
$$\overline{200\,\mathrm{m}}$$

Figure 3: Single leaky pipe of length $\ell = 1500\,\mathrm{m}$, connecting a tank ■ to a junction ●.

2.4.4. WDN with highly contrasted values of flow rates and/or pressures

At each Newton iteration m, the magnitude of the elements in $\boldsymbol{J}^{(m)}$ depends strongly on the values of $\boldsymbol{q}_{0.5}^{(m)}$ and $\boldsymbol{h}^{(m)}$ (see section 2.2.3). However, in a WDN, the values in $\boldsymbol{q}_{0.5}^{(m)}$ and $\boldsymbol{h}^{(m)}$ may be very different from one part of the WDN to another, according, e.g., to user demands, tank levels, use of pumps and/or valves, etc. In such cases, using $\boldsymbol{J}^{(m)}$ as it could lead to convergence errors.

To prevent these errors, we adapt the preconditioning method initially proposed by [8], so it now deals with user consumptions and background leakages depending on pressure too.

2.4.5. Initial guesses far from the solution

Finally, the bottleneck of the Newton algorithm is the resolution, at each iteration, of the linear system (44). But this algorithm can need numerous iterations if the initial guesses of flow rates at middle of pipes and heads at junctions are far from the solutions at equilibrium. In this case, the simulation of large WDNs could become unfeasible in reasonable computation time.

To deal with such situation, we choose to reuse the damping algorithm initially proposed by [9], extending it so it now takes pressure-dependent background leakages into account too.

2.5. Checking and comparison

In this sub-section, we describe the test cases used to check and compare the models M0, M1, M2, M3 and Ref. We also propose a method to estimate the convergence order of the discretization algorithm used in model Ref. Finally, we show how to compute the total background leakage outflow in each pipe of a WDN.

2.5.1. Test cases

The first test case aims at checking for the good functioning and stability of the models for a very simple network. Thereby, this test consists in simulating a single leaky pipe of length $\ell = 1500\,\mathrm{m}$, connecting one tank to one junction, both located at the ground level (fig. 3). The junction has a demand $d = 10\,\mathrm{l\,s^{-1}}$, and the tank has a fixed head $h_t = 10\,\mathrm{mH_2O}$. The pipe has a diameter $\varnothing = 200\,\mathrm{mm}$, a Hazen-Williams friction coefficient $C_{HW} = 120$, background leakages of type $\alpha = 1.5$, and a level of degradation $\beta = 10^{-3}\,\mathrm{l\,s^{-1}\,m^{-1-\alpha}}$. These values of $\{\alpha, \beta\}$ correspond to a very high level of leakages, and are chosen to magnify the differences between the leakage models. Finally, this first test case explores the potential of models $\{M0, M1, M2, M3\}$ to adjust the model Ref, using a classical calibration method described in the supplementary material. The Epanet2 and leakages input files of the network are also available in the supplementary material (files `SinglePipe_Epanet2.inp` and `SinglePipe_Leakages.csv`).

Next, through a second test case, we propose to compare the models M0, M1, M2, M3 and Ref on a bigger network derived from a real leaky WDN. To do so, we simulate the network C-Town, already used by [13, 21] (fig. 1). We set the demands $\boldsymbol{d}$ at junctions to half of the nominal demands, which leads to a mean demand $\bar{d} = 0.35\,\mathrm{l\,s^{-1}}$. The pumps and the valve are all closed, because the initial levels of the water in tanks are all positive. The Epanet2 input file of the network is available in the supplementary material (file `C-Town_Epanet2.inp`). For background leakages parameters $\{\boldsymbol{\alpha}, \boldsymbol{\beta}\}$, we first use the same values as in [13], such that $\alpha_k = 0.9$ and $\beta_k \in \{1, 2, 4\} \times 10^{-5}\,\mathrm{l\,s^{-1}\,m^{-1-\alpha}}, \forall k \in \{1..n_p\}$; the corresponding leakages file is also provided as supplementary material (`C-Town_Leakages.csv`). Next, to find the range of applications of the different models according to the degradation level of the pipes, we successively use, for all pipes, a value of β going from 10^{-7} to $10^{-2}\,\mathrm{l\,s^{-1}\,m^{-1-\alpha}}$, while maintaining $\alpha_k = 0.9 \,\forall k \in \{1..n_p\}$.

For both test cases, we use minimal pressure-heads $p_m = 0\,\mathrm{mH_2O}$ and service pressure-heads $p_s = 20\,\mathrm{mH_2O}$. Also, all simulations are run on an Intel Core i9 with 32 GB of memory, and all computations are done in double-precision.

2.5.2. Order of convergence

To quantify the efficiency of the discretization algorithm used in model Ref, we compute its order of convergence. To do so, we denote $\boldsymbol{h}_{\boldsymbol{N}}^{(s_c+1)}$ the HGL at the iteration $s_c + 1$ of the discretization algorithm, and, $\forall s \in \{1..s_c\}$, we denote $\widetilde{\boldsymbol{h}_{\boldsymbol{N}}^{(s)}}$ the HGL at iteration s interpolated at the same positions as $\boldsymbol{h}_{\boldsymbol{N}}^{(s_c+1)}$. Then, denoting $\varepsilon^{(s)} = \left\| \boldsymbol{h}_{\boldsymbol{N}}^{(s_c+1)} - \widetilde{\boldsymbol{h}_{\boldsymbol{N}}^{(s)}} \right\|_\infty$ the infinity norm between $\boldsymbol{h}_{\boldsymbol{N}}^{(s_c+1)}$ and $\widetilde{\boldsymbol{h}_{\boldsymbol{N}}^{(s)}}$, the order of convergence η of our discretization algorithm is defined from the relation

$$\varepsilon^{(s)} = a\, s^{\eta}, \tag{53}$$

with a a constant. Thus, to estimate η, we first compute $\varepsilon^{(s)} \; \forall s \in \{1..s_c\}$. Next we rewrite eq. (53) in log‑log scale as

$$\left|\log(\varepsilon^{(s)})\right| = \log(a) + \eta \log(s). \tag{54}$$

Finally, we compute η by linear regression of eq. (54).

2.5.3. Derived leakage outflow

Models M0, M1, M2, M3 and Ref permit to approximate the functions $q_{LL}^{theo}(x)$ (eq. (3)), $q^{theo}(x)$ (eq. (4)) and $\xi^{theo}(x)$ (eq. (6)). But, to obtain a more explicit indicator of the level of background leakages in each pipe, we also compute, for each model, the total leakage outflow as

$$q_L = |q_\ell - q_0|, \tag{55}$$

where q_0 and q_ℓ are the flow rates at respectively the start and the end of the pipe.

For the second test case (see section 2.5.1), we obtain the vector of background leakage outflows $\boldsymbol{q_L} = \left(q_{L,1}, .., q_{L,n_p}\right)^T \in \mathbb{R}^{n_p}$. To compare the models at the global scale, we then compute the 1-norm of $\boldsymbol{q_L}$.

We suppose that the difference between the q_L or 1-norm computed with two different models becomes significant when it is greater than $10^{-2}\,\mathrm{l s}^{-1}$. Indeed, this threshold corresponds to the best precision one can expect from physical measurements [19, 26, 33].

2.6. Implementation and framework

We implement our models in Python[1], using the Anaconda distribution[2]. At each Newton iteration, we solve the linear system (44) using the sparse solver UMFPACK [6] through its SciPy [31] interface[3]. Also, in the discretization algorithm of model Ref, we use the PCHIP interpolator[4] from SciPy.

Also, we choose to integrate all our developments into the framework OOPNet, which provides convenient way to read Epanet input files and to convert them to object oriented data structures [27, 28].

3. Results and discussion

We present here the results obtained from the test cases presented in section 2.5.1. For each test case, we first check the functioning of the discretization algorithm. Next, we discuss the execution times of each model. Finally, we compare the models between each other.

For the first test case only (i.e., the single leaky pipe), we also compare the results of the models {M0, M1, M2, M3} after the calibration of their leakage parameters using the method described in the supplementary material, supposing that the measured data needed for the calibration are equal to the results of the Ref model. Like so, we explore the potential of models {M0, M1, M2, M3} to adjust model Ref.

3.1. First test case: single leaky pipe

This first test case, that corresponds to the simulation of a single leaky pipe, is a useful and simple benchmark to verify the accuracy and stability of proposed models.

3.1.1. Discretization algorithm

For this test case, the discretization algorithm needs 6 iterations to find the reference HGL $\boldsymbol{h}_N^{Ref} = \boldsymbol{h}_N^{(5)}$ (fig. 4). We can see that new sub-pipes and intermediate junction nodes are created at each iteration (figs. 4a to 4e). Also, as expected, the discretization is irregular. For example, at iteration 6 the number of sub-pipes is equal to 58 (fig. 4e) while at iteration 5 it is equal to 31 (fig. 4d). This signifies that 2 of the 31 sub-pipes from iteration 5 have not been rediscretized because they did not need it.

At convergence, the pipe is discretized in 31 sub-pipes (fig. 4d). This high number of needed sub-pipes can be explained by the strong values of the leakage parameters used. The order of convergence is equal to 3.10 (fig. 4f), which is more than cubic and so very good. The CPU time elapsed during the discretisation process is equal to 330 ms. This is quick, but normal when simulating a single pipe.
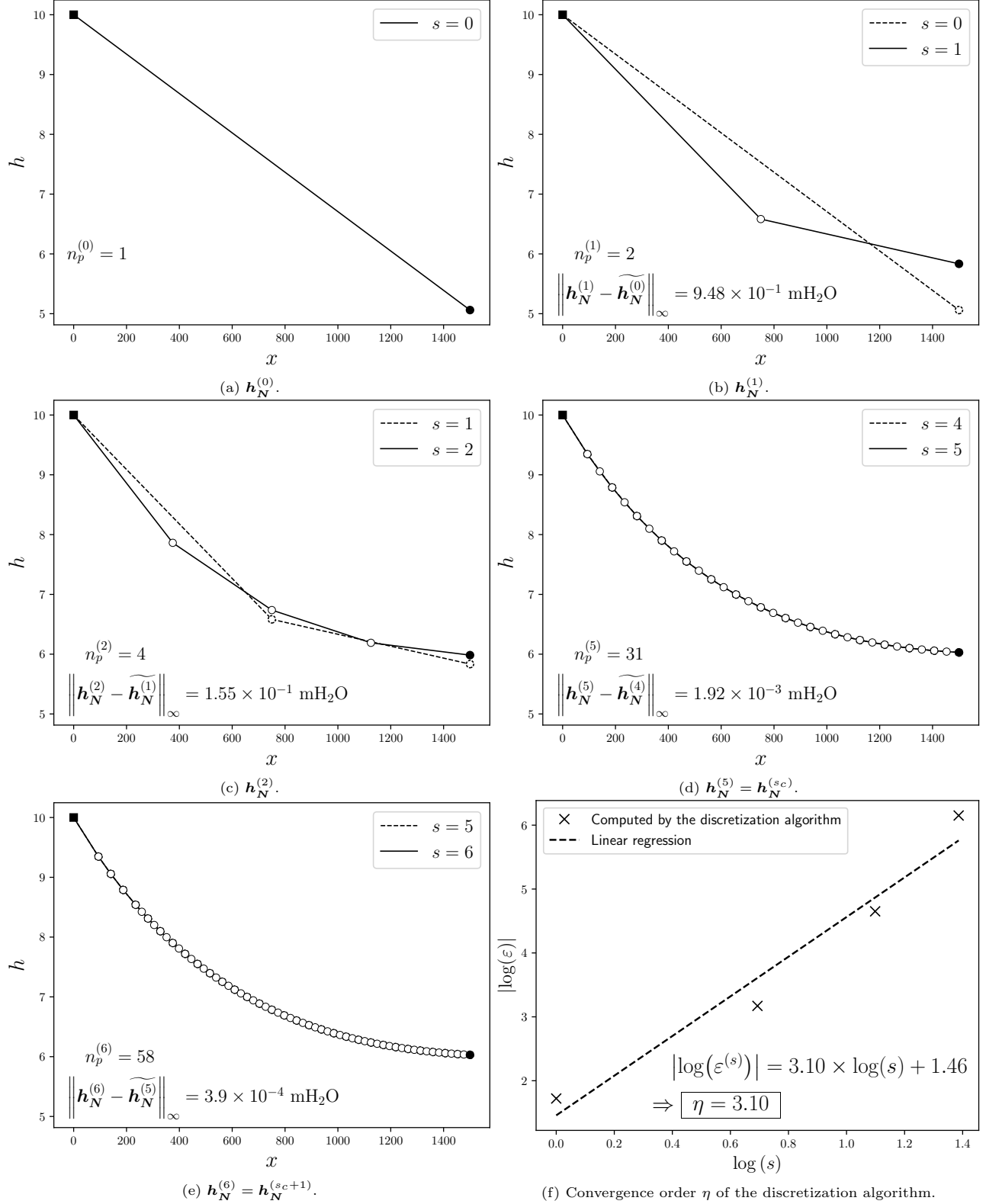

Figure 4: Evolution of the hydraulic grade line (HGL) $\boldsymbol{h}_N^{(s)}$ (figs. 4a to 4e), and convergence order η (fig. 4f), when applying the discretization algorithm of model Ref to the single leaky pipe of fig. 3. h: head (in mH$_2$O) at position $x \in [0,\ell]$ (in m) along the pipe. $s \in \{0..s_c + 1\}$: iteration of the discretization algorithm ($s = 0$: initial state, $s = s_c$: convergence). $n_p^{(s)}$: number of sub-pipes at iteration s. $\widetilde{\boldsymbol{h}_N^{(s)}}$: HGL at iteration s, interpolated at positions of $\boldsymbol{h}_N^{(s+1)}$. $\varepsilon^{(s)}$: infinity norm between $\boldsymbol{h}_N^{(s_c+1)}$ and $\widetilde{\boldsymbol{h}_N^{(s)}}$. $\widetilde{\boldsymbol{h}_N^{(s)}}$: HGL at iteration s interpolated at positions of $\boldsymbol{h}_N^{(s_c+1)}$ (see section 2.5.2 for deeper explanations).

Finally, replacing the use of model M0 by the one of M1, M2 or M3 in the discretization algorithm leads to the same HGL at convergence. Thus, the algorithm remains stable whatever the model we use, and all models M0, M1, M2 and M3 give equivalent results providing that the pipe is discretized in enough sub-pipes. These results were expected because all the functions used internally in the models are continuous.

3.1.2. Execution times

The simulation of the leaky pipe lasts respectively $25\,\mathrm{ms}$ with M0, $35\,\mathrm{ms}$ with M1, $50\,\mathrm{ms}$ with M2, $66\,\mathrm{ms}$ with M3, and $367\,\mathrm{ms}$ with Ref. Thus, we can clearly see that our new models M1, M2, M3 and Ref need more time than the state of the art one, but this is normal because the equations in our new models are more complex. Also, we can see that the increase of computation time is relative to the complexity of the models.

Model Ref is naturally much more time consuming than other models because it consists in running internally 6 times the model M0, on more and more discretized networks, and because it needs PCHIP interpolation between each of these internal runs. The difference between the elapsed time of the discretization algorithm ($330\,\mathrm{ms}$; see section 3.1.1), and the total elapsed time of the model Ref ($367\,\mathrm{ms}$), is equal to $367 - 330 = 37\,\mathrm{ms}$ ($\approx 10\ \%$ of the total elapsed time), and corresponds to the post-processing needed to aggregate and interpolate the heads and flow rates in the discretized pipe at convergence to the head and flow rate at the undiscretized pipe scale. Finally, the simulation of the leaky pipe with model Ref remains less than half of a second, which is an acceptable time, especially since we are using the interpreted language Python.

3.1.3. Comparison of the models before calibration

The drawn profiles of functions $\left\{\mathrm{q}_{\mathrm{LL}}^i(x), \mathrm{q}^i(x), \mathrm{h}^i(x)\right\}$, $i \in \{\mathrm{Ref}, \mathrm{M0}, \mathrm{M1}, \mathrm{M2}, \mathrm{M3}\}$ are consistent with the degrees of each model (figs. 5a, 5c and 5e). Indeed, since we use model M0 in the discretization algorithm, it is normal that $\mathrm{q}_{\mathrm{LL}}^{\mathrm{Ref}}(x)$ and $\mathrm{q}^{\mathrm{Ref}}(x)$ are step functions. Also, as expected, $\mathrm{q}_{\mathrm{LL}}^{\mathrm{M0}}(x)$ and $\mathrm{q}_{\mathrm{LL}}^{\mathrm{M1}}(x)$ are constant along the full pipe, $\mathrm{q}_{\mathrm{LL}}^{\mathrm{M2}}(x)$ is affine, and $\mathrm{q}_{\mathrm{LL}}^{\mathrm{M3}}(x)$ is slightly convex. Finally, $\forall i \in \{\mathrm{Ref}, \mathrm{M0}, \mathrm{M1}, \mathrm{M2}, \mathrm{M3}\}$, $\mathrm{h}^i(x)$ logically starts from the fixed head at tank $h_t = 10\,\mathrm{mH_2O}$. Globally, we can see that the higher the degree of the model is, the better the curves from $\{\mathrm{M0}, \mathrm{M1}, \mathrm{M2}, \mathrm{M3}\}$ fit the ones from model Ref.

The absolute errors on $\left\{q_{LLx}^i, q_x^i, h_x^i\right\}$ when compared to $\left\{q_{LLx}^{\mathrm{Ref}}, q_x^{\mathrm{Ref}}, h_x^{\mathrm{Ref}}\right\}$, $x \in \{0, \ell/2, \ell\}$, are generally smaller for the new models $\{\mathrm{M1}, \mathrm{M2}, \mathrm{M3}\}$ than for the state of the art model M0 (figs. 5b, 5d and 5f). For example, from model M0 to models M1, M2 and M3, the errors on $q_{LL\ell}^i$ decrease (in absolute value) by respectively $11.30\ \%$, $64.80\ \%$ and $69.20\ \%$, and the ones on $h_{\ell/2}^i$ by respectively $19.40\ \%$, $31.10\ \%$ and $40.30\ \%$. However, at some positions, some of the new models $\{\mathrm{M1}, \mathrm{M2}, \mathrm{M3}\}$ give worse results than M0. In particular, the error on h_ℓ^i increases (in absolute value) by $58.80\ \%$ from M0 to M1. But these greater error is weighed against the smaller ones on $q_{LL\ell/2}^{\mathrm{M1}}$ ($-21.00\ \%$) and $q_{LL\ell/2}^{\mathrm{M1}}$ ($-82.90\ \%$). Finally, model M3 gives generally better results than M2, which gives itself better results than M1. This order is consistent with the increasing complexity of models $\{\mathrm{M0}, \mathrm{M1}, \mathrm{M2}, \mathrm{M3}\}$.

3.1.4. Comparison of the models after calibration

We present here the results of the models $\{\mathrm{M0}, \mathrm{M1}, \mathrm{M2}, \mathrm{M3}\}$ after the calibration of their leakage parameters, and compare them against the results of model Ref.

Globally, the calibrated leakage parameters α^i, $i \in \{\mathrm{M2}, \mathrm{M3}\}$ (α cannot be calibrated for $\{\mathrm{M0}, \mathrm{M1}\}$), are very close to the uncalibrated α. Conversely, the calibrated β^i, $i \in \{\mathrm{M0..M3}\}$, differ much from β (fig. 6). Indeed, the relative errors on α when compared to α^i are equal to $\sim 2\ \%_{00}$, while the relative errors on β when compared to β^i are all more than $22\ \%$. Thus we can say, for this test case, that β is much more sensitive than α to the leakage model in use. Also, we observe a greater error on β for M1 ($34.60\ \%$) than for $\{\mathrm{M0}, \mathrm{M2}, \mathrm{M3}\}$ (between $22.30\ \%$ and $24.10\ \%$). This is probably due to the impossibility to calibrate α for M1, while constraining its flow rate $\mathrm{q}^{\mathrm{M1}}(x)$ to pass through q_ℓ^{Ref}. In other words, for M1 the calibration of β has to compensate for the absence of calibration of α.

Using models $\{\mathrm{M0..M3}\}$ with calibrated leakage parameters, the drawn profiles of the functions $\left\{\mathrm{q}_{\mathrm{LL}}^i(x), \mathrm{q}^i(x), \mathrm{h}^i(x)\right\}$ follow the same tendencies before calibration. But, as expected, the curves of the calibrated functions now fit more closely the reference ones $\left\{\mathrm{q}_{\mathrm{LL}}^{\mathrm{Ref}}(x), \mathrm{q}^{\mathrm{Ref}}(x), \mathrm{h}^{\mathrm{Ref}}(x)\right\}$ (figs. 7a, 7c and 7e). In particular, $\mathrm{h}^i(x)$ now passes (or almost passes) through h_ℓ^{Ref} $\forall i \in \{\mathrm{M0..M3}\}$ (fig. 7e). This gain in accuracy is even more visible for models $\{\mathrm{M2}, \mathrm{M3}\}$, for which both leakage parameters α and β are calibrated. Indeed, $\mathrm{q}^{\mathrm{M2}}(x)$ and $\mathrm{q}^{\mathrm{M3}}(x)$ now passes through q_0^{Ref} and q_ℓ^{Ref} (fig. 7c).

As expected, the calibration of the leakage parameters leads to bigger reductions of the absolute errors on q_0 for models $\{\mathrm{M2}, \mathrm{M3}\}$: $-98.90\ \%$ for M2 (vs. $-64.90\ \%$ before calibration) and $-99.10\ \%$ for M3 (vs. $-68.40\ \%$ before calibration) (see fig. 7d). Likewise, the calibration drives to stronger reductions of the errors on $h_{\ell/2}$ $\forall i \in \{\mathrm{M1}, \mathrm{M2}, \mathrm{M3}\}$: $-87.50\ \%$ for M1 (vs. $-19.40\ \%$ before calibration), $-97.30\ \%$ for M2 (vs. $-31.10\ \%$ before calibration), and $-96.80\ \%$ for M3 (vs. $-40.30\ \%$ before calibration) (see also fig. 7f). This last result is particularly interesting since it demonstrates that, unlike the existing model M0 from [12], our new models compute after calibration much better estimations of head at intermediate positions along the pipe (here at $x = \ell/2$) than before calibration. Thus, using our new models $\{\mathrm{M1}, \mathrm{M2}, \mathrm{M3}\}$ could probably reduce significantly the number of measuring points and sensors needed to get an exhaustive and accurate HGL along the pipe, especially once the models are calibrated.
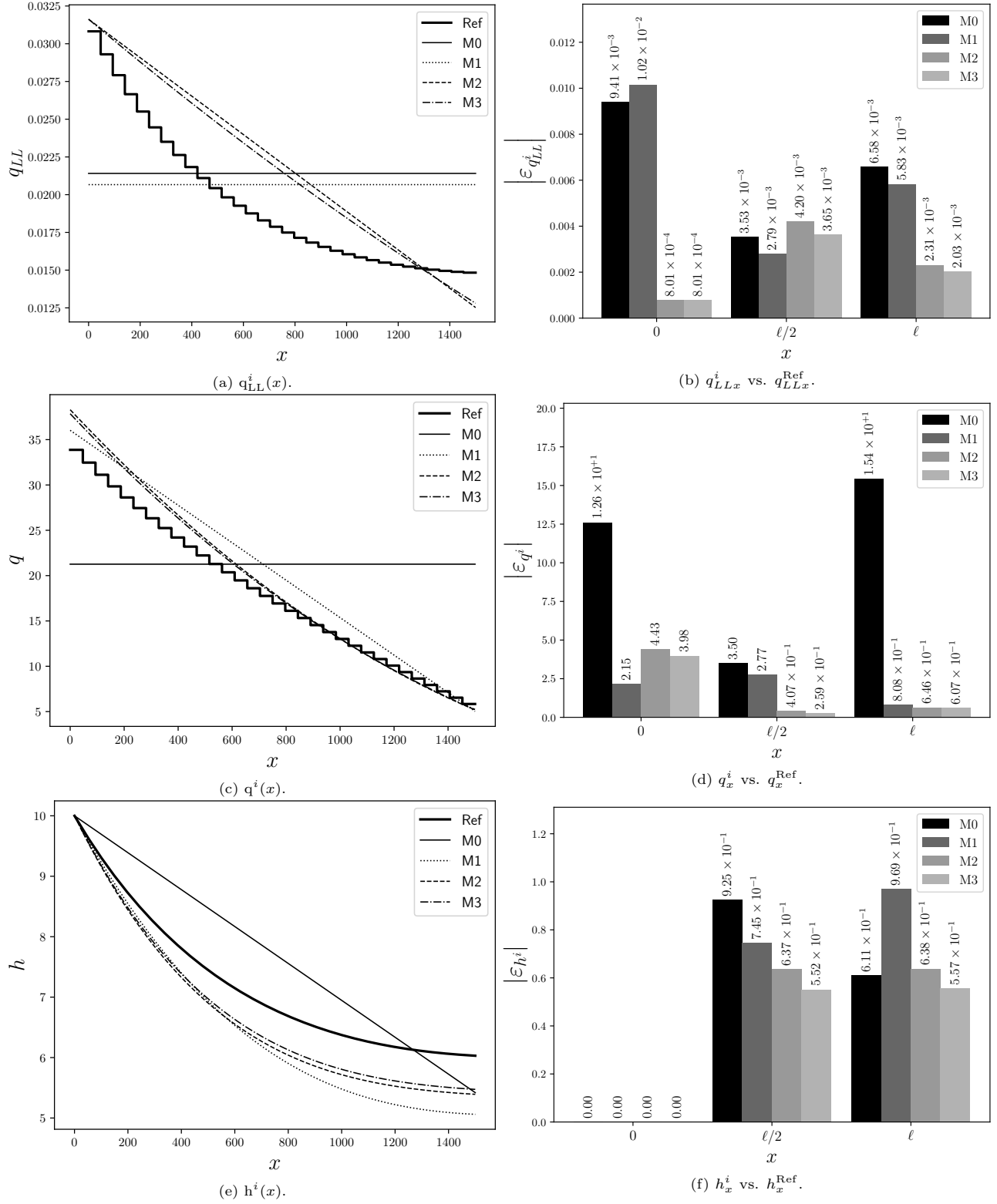
(a) $q_{LL}^i(x)$.

(b) q_{LLx}^i vs. q_{LLx}^{Ref}.

(c) $q^i(x)$.

(d) q_x^i vs. q_x^{Ref}.

(e) $h^i(x)$.

(f) h_x^i vs. h_x^{Ref}.

Figure 5: Lineic leakage outflows q_{LL}^i (in $\mathrm{l\,s^{-1}\,m^{-1}}$), flow rates q^i (in $\mathrm{l\,s^{-1}}$) and heads h^i (in $\mathrm{mH_2O}$) along the leaky pipe of fig. 3, for each model $i \in \{\mathrm{Ref}, \mathrm{M0}, \mathrm{M1}, \mathrm{M2}, \mathrm{M3}\}$, using the same uncalibrated leakage parameters $\alpha = 1.5$ and $\beta = 10^{-3}\,\mathrm{l\,s^{-1}\,m^{-1-\alpha}}$ for all models; these parameters correspond to a very high level of leakages, and are chosen to magnify the differences between the models. Figures 5a, 5c and 5e show the profiles of the functions. Figures 5b, 5d and 5f show the absolute errors between models $\{\mathrm{M0}, \mathrm{M1}, \mathrm{M2}, \mathrm{M3}\}$ and Ref, at positions $x \in \{0, \ell/2, \ell\}$, $\ell = 1500\,\mathrm{m}$.
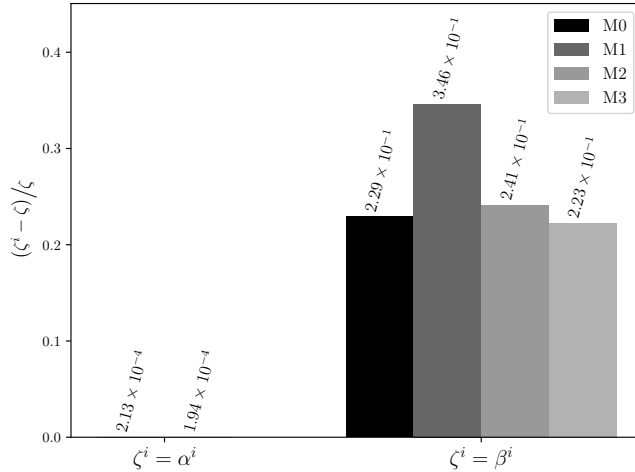
Figure 6: Relative difference (unit-less) between the uncalibrated leakage parameters $\zeta \in \{\alpha, \beta\}$, and the calibrated ones $\zeta^i \in \{\alpha^i, \beta^i\}$ obtained from the flows and heads computed by the model Ref, for the leaky pipe of fig. 3. For α^i: $i \in \{M2, M3\}$ (not possible to calibrate parameter α for models $\{M0, M1\}$). For β^i: $i \in \{M0, M1, M2, M3\}$.

Finally, for each of $\{M0, M1, M2, M3\}$, when we gain precision by means of calibration for some variables at some locations, we also loose some precision on other variables and at other locations (e.g., q^i_{LLx} on fig. 7b). This is unavoidable since, even if more accurate, our new models remain approximations of the theoretical model.

3.2. Second test case: network C-Town

This second test case is proposed in order to validate the functioning, accuracy and stability of our models when simulating a larger and more realistic network. For this purpose, we choose network C-Town [13, 21], which includes most of the critical parameters needed for validation, while still remaining compact enough to perform quick simulations.

3.2.1. Discretization algorithm

For the network C-Town (fig. 1), our discretization algorithm needs 4 iterations and 12.99 s of CPU time to find the reference HGL $\boldsymbol{h}_N^{\mathrm{Ref}} = \boldsymbol{h}_N^{(3)}$. This longer elapsed time is explained by the high number of pipes and/or sub-pipes to simulate as the network is discretized. Indeed, the discretized networks consist of $n_p^{(1)} = 819$, $n_p^{(2)} = 1590$, $n_p^{(3)} = 1824$ and $n_p^{(4)} = 1832$ pipes and/or sub-pipes at respectively iteration 1, 2, 3 and 4.

Also, none of $\left\{n_p^{(1)}, n_p^{(2)}, n_p^{(3)}, n_p^{(4)}\right\}$ is a multiple of the initial number of pipes $n_p^{(0)} = 432$, which means that the network is discretized irregularly (i.e., some pipes are more discretized than some others) at each iteration. As a reminder, this irregular discretization prevents from over-discretization of pipes presenting low gradients of pressures, and permits to speed-up the computations.

The order of convergence of the discretization algorithm is equal to 1.66 (fig. 4f). This means that our discretization algorithm remains efficient even when applied to a real network with many pipes.

Finally, as for the first test case, replacing model M0 by M1, M2 or M3 in the discretization algorithm leads to the same HGL. Thus, the algorithm remains stable whatever the model we use, providing that the pipes are discretized in enough sub-pipes.

3.2.2. Execution times

The simulation of the network C-Town lasts respectively 0.19 s with M0, 0.32 s with M1, 0.41 s with M2, 0.45 s with M3, and 16.18 s with Ref. As in the first test case, we can clearly see that our new models, especially the Ref one, need more time than M0. But this is normal because our models are more complex and accurate.

Also, the difference between the elapsed time of the discretization algorithm (12.99 s; see section 3.2.1), and the total elapsed time of the model Ref (16.18 s), is equal to $16.18 - 12.99 = 3.19$ s (≈ 20 % of the total elapsed time), and corresponds to the post-processing needed to aggregate and interpolate the heads and flow rates in the discretized network at convergence to the heads and flow rates at the undiscretized network scale. For current test case, the elapsed time due to post-processing is proportionally two times greater than the one found in the first test case (i.e., ≈ 10 %). This can be explained by the greater number of iterations needed in the first test case, and by the greater number of pipes in the second test case (the post-processing is done sequentially pipe after pipe).

Nevertheless, all these execution times remain acceptable, and could be probably reduced by re-implementing the simulator using a compiled language, and/or parallelizing the post-processing at the end of the discretization algorithm. However, for some applications like sensitivity analysis, for which many runs are needed, the models M0, M1, M2 and M3 should be preferred to model Ref in terms of rapidity.
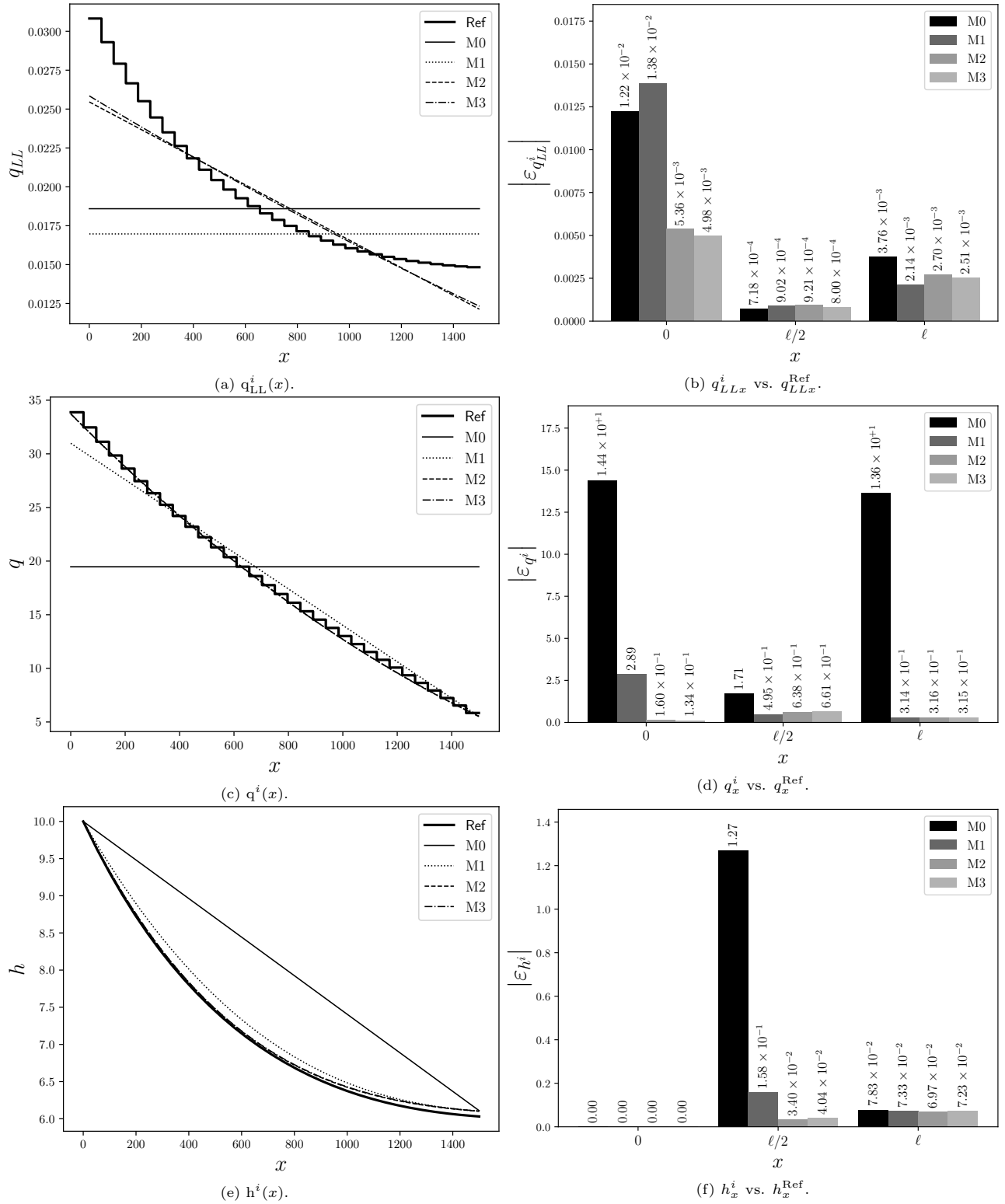
(a) $q_{LL}^i(x)$.

(b) q_{LLx}^i vs. q_{LLx}^{Ref}.

(c) $q^i(x)$.

(d) q_x^i vs. q_x^{Ref}.

(e) $h^i(x)$.

(f) h_x^i vs. h_x^{Ref}.

Figure 7: Lineic leakage outflows q_{LL}^i (in $\mathrm{l\,s^{-1}\,m^{-1}}$), flow rates q^i (in $\mathrm{l\,s^{-1}}$) and heads h^i (in $\mathrm{mH_2O}$) along the leaky pipe of fig. 3, for each model $i \in \{\mathrm{Ref, M0, M1, M2, M3}\}$. For $\{\mathrm{M0, M1, M2, M3}\}$, the leakage parameters calibrated from the flows and heads computed by the model Ref are used. Figures 7a, 7c and 7e show the profiles of the functions. Figures 7b, 7d and 7f show the absolute errors between models $\{\mathrm{M0, M1, M2, M3}\}$ and model Ref, at positions $x \in \{0, \ell/2, \ell\}$, $\ell = 1500\,\mathrm{m}$.
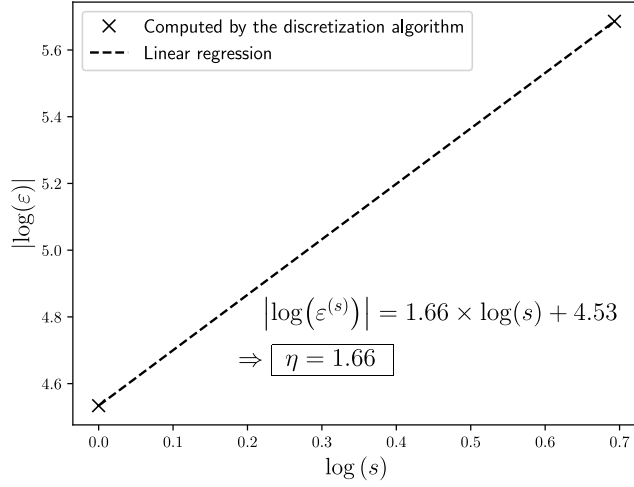
Figure 8: Computation of the convergence order η of the discretization algorithm when applied to network C-Town (fig. 1). $s \in \{0..s_c + 1\}$: iteration of the discretization algorithm ($s = 0$: initial state, $s = s_c$: convergence). $\varepsilon^{(s)}$: infinity norm between the hydraulic grade lines (HGLs) at $s \in \{1..s_c\}$ and the one at $s = s_c + 1$.
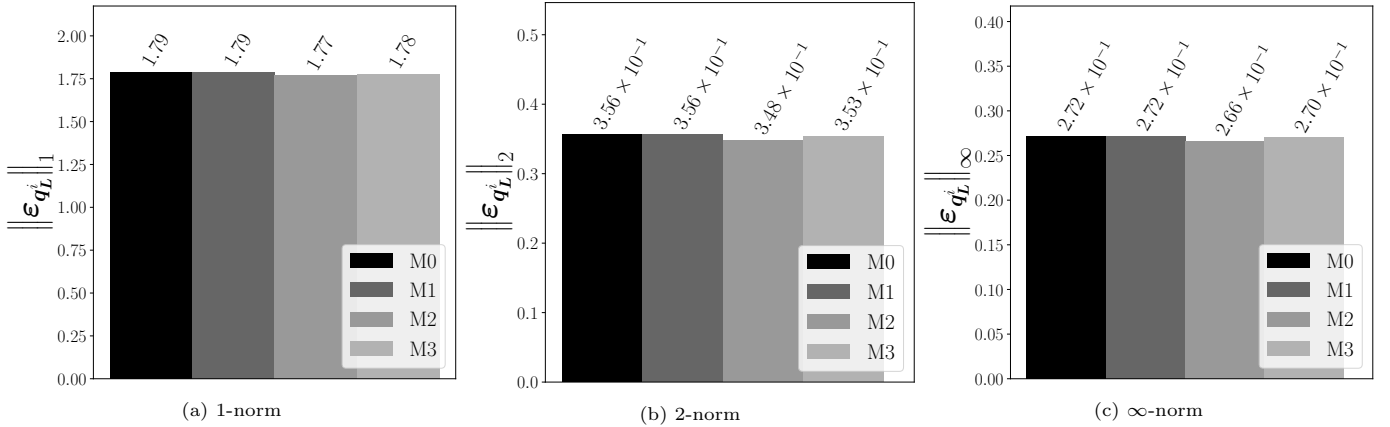

Figure 9: p-norm, $p \in \{1, 2, \infty\}$, of the absolute errors $\boldsymbol{\varepsilon}$ between the leakage outflows $\boldsymbol{q_L^i}$ (in $1s^{-1}$) computed from each model $i \in \{M0, M1, M2, M3\}$ and the ones computed with model Ref.

3.2.3. Comparison of the models

The 1-norms of the errors between the leakage outflows computed with models $\{M0, M1, M2, M3\}$ and the ones computed with model Ref vary from $1.771 s^{-1}$ to $1.791 s^{-1}$ (fig. 9a). The 2 and ∞-norms of these errors are respectively around $0.351 s^{-1}$ and $0.271 s^{-1}$ (figs. 9b and 9c). Thus, the leakage outflows computed by models $\{M0, M1, M2, M3\}$ are very close to each other, but they are also significantly different from the ones computed with model Ref. Indeed, supposing that the pressures and the demands remain the same during all a day, then these differences represent $1.78 \times 3600 \times 24 = 153.79 \, \text{m}^3$ per day, and thus more than the daily consumption of 1000 inhabitants in France [18].

The small differences between models $\{M0, M1, M2, M3\}$ can be explained by the characteristics of the network C-Town. Indeed, C-Town has low deltas of elevation along its pipes: a median equals to $3.06 \, \text{m}$, and an IPR (inter percentile range) between percentiles 10th and 90th equals to $13.71 \, \text{m}$. Since the pressures are directly correlated to the elevations (i.e., $p = h - u$), the deltas of pressure induced by these deltas of elevation are low too. Thus, we believe that he gradients of pressure in C-Town is enough for seeing differences between models $\{M0, M1, M2, M3\}$ and Ref, but barely enough to observe differences between M0, M1, M2, M3. Still, supposing that the pressures and the demands remain the same during all a day, the differences between M0 and M3 represent $0.02 \times 3600 \times 24 = 1.73 \, \text{m}^3$ per day, which already shows a little improvement from M0 to M3. Moreover, we think, by analogy with the first test case, that the leakage outflows computed from models $\{M0, M1, M2, M3\}$ would show more difference with the use for each of them of specifically calibrated leakage parameters. But we do not have, at the time of this study, the measured data which would permit us to calibrate these parameters.

But, first of all, these small differences are due to the low degradation levels (i.e., $\beta_k \in \{1, 2, 4\} \times 10^{-5} \, 1s^{-1} \, \text{m}^{-1-\alpha}$) chosen by [13]. Indeed, when using successively, for all pipes of the network C-Town, a single value of β varying from 10^{-7} to $10^{-2} \, 1s^{-1} \, \text{m}^{-1-\alpha}$ [2, 19], we can then observe much larger differences between the models (table 1). In particular, we can clearly see on table 2 that the models M0 and M1, which do not depend on the gradient of pressure, are more accurate

19

for very low degradation levels (i.e., $\leq 10^{-6}\,\mathrm{l\,s^{-1}\,m^{-1-\alpha}}$), and that models M2 and M3, which depend on the gradient of pressure, are more accurate for medium and high degradation levels (i.e., $\geq 10^{-5}\,\mathrm{l\,s^{-1}\,m^{-1-\alpha}}$); this was expected because higher values of β make naturally decreases quicker the pressure along the pipes, leading to stronger errors when the gradient of pressure is neglected. Moreover, we notice on table 2 that, for very low degradation levels, the absolute differences between the worst and the best models are no more than $0.07\,\mathrm{m^3}$ per day; thus, even if the models M0 and M1 show better results for these degradation levels, the differences with models M2 and M3 are in this case barely significant. Also, for each degradation level β, we can see that the worst and the best models differ by $\sim 3\,\%$, and that higher β lead to higher relative differences, up-to $4.14\,\%$ for $\beta = 10^{-2}\,\mathrm{l\,s^{-1}\,m^{-1-\alpha}}$ (column "Rel. Diff." of table 2). Finally, the model M3 is often the best one and never the worst one; this means that M3 could probably be used efficiently in most circumstances.

Table 1: 1-norm of the absolute errors $\boldsymbol{\varepsilon}$ between the leakage outflows $\boldsymbol{q_L^i}$ (in $\mathrm{m^3}$ per day) computed from each model $i \in \{\mathrm{M0}, \mathrm{M1}, \mathrm{M2}, \mathrm{M3}\}$ and the ones computed with model Ref, for different degradation levels of pipes β (in $\mathrm{l\,s^{-1}\,m^{-1-\alpha}}$).

β	M0	M1	M2	M3
10^{-7}	0.34	0.34	0.35	0.34
10^{-6}	3.43	3.43	3.50	3.45
10^{-5}	49.55	49.55	49.07	49.21
10^{-4}	384.38	384.15	376.63	379.23
10^{-3}	12,209.60	12,210.74	12,268.77	11,912.84
10^{-2}	62,589.03	62,819.85	62,375.31	60,322.17

Table 2: Comparison of the models when simulating leakage outflows in network C-Town of second test case for different degradation levels β (in $\mathrm{l\,s^{-1}\,m^{-1-\alpha}}$). The "Best model" is the one that has the lowest 1-norm of absolute errors when compared to model Ref; this 1-norm is reported in column "Best vs. Ref [...]" (in $\mathrm{m^3}$ per day). Conversely, the "Worst model" has the highest 1-norm of absolute errors. In the column "Worst vs. Best", the sub-column "Abs. Diff." shows the absolute difference (in $\mathrm{m^3}$ per day) between the worst and the best models for each β, and the sub-column "Rel. Diff." presents the relative differences (in %) computed as: (worst - best) / best $\times$ 100. The 1-norms of all models for all β are listed in table 1.

β	Best model	Best vs. Ref Norm 1	Worst model	Worst vs. Best	
				Abs. Diff.	Rel. Diff.
10^{-7}	M0	0.34	M2	0.01	2.08
10^{-6}	M1	3.43	M2	0.07	2.04
10^{-5}	M2	49.07	M0	0.49	0.99
10^{-4}	M2	376.63	M0	7.74	2.06
10^{-3}	M3	11,912.84	M2	355.93	2.99
10^{-2}	M3	60,322.17	M1	2,497.68	4.14

The 1-norm of the errors made by the best model among M0, M1, M2 and M3, when compared to the model Ref, varies almost linearly with the value of the degradation level β (fig. 10). Thus, for very high β, the Ref discretization model, even if more time consuming, should be preferred to any of $\{\mathrm{M0}, \mathrm{M1}, \mathrm{M2}, \mathrm{M3}\}$ to obtain accurate results.

The results presented in this section indicate the range of applications of the different models according to the degradation level of the pipes in a real leaky network. They demonstrate the superiority of our new models M1, M2, M3 and Ref over the pre-existing M0, for medium to high levels of leakages, and so even for low deltas of elevation along the pipes. For low levels of leakages, the differences between the models are not significant; the models are then equivalent.

4. Conclusions

In this study, we demonstrated, through two complementary test cases, the interest in using more complex PDM models of background leakages in WDNs. This statement relies on the comparison of a state of the art model to new more accurate models. These new models were developed from successive original refinements of the state of the art one, or through the recursive discretization of the pipes into sub-pipes until the HGL along each pipe converges. The choice between our new models depends on the exhaustiveness of the measured data needed to calibrate them, on the level of accuracy to reach, and on the a priori degradation level of the pipes (estimated, e.g., from the age of the pipes).

Among our new models, the one based on the recursive discretization of the pipes leads to reference background leakage outflows, flow rates and friction head-losses which are very close to the ones we would obtain if we knew the exact pressures all along the pipes. This algorithm could be easily reused to test other WDN models, or adapt to any graph structured model from different fields of applied mathematics and scientific computation.
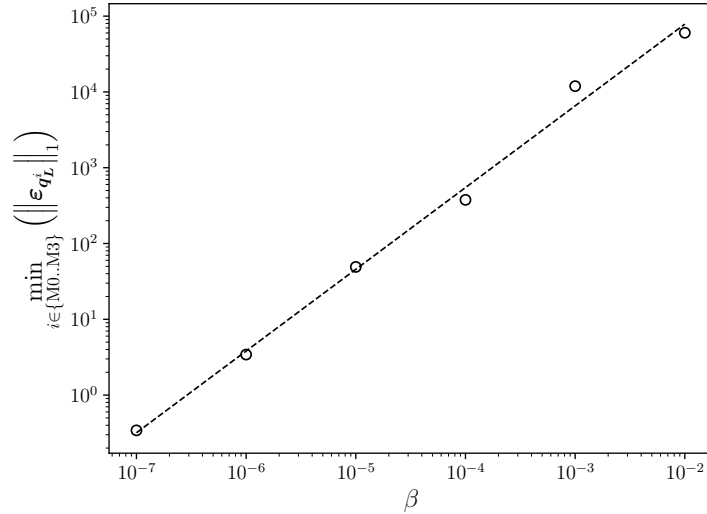
Figure 10: Relation between the degradation level of pipes, β (in $\mathrm{l\,s^{-1}\,m^{-1-\alpha}}$), and the 1-norm of the errors made by the best model among M0, M1, M2 and M3 when compared to the model Ref, $\min\limits_{i\in\{\mathrm{M0..M3}\}}\left(\left\|\boldsymbol{\varepsilon}_{\boldsymbol{q}_L^i}\right\|_1\right)$ (in $\mathrm{m^3}$ per day), during the simulation of the leakage outflows in the network C-Town of the second test case. Both abscissa and ordinate axes are in log-log scale.

By taking into account of the gradient of pressure-heads along the pipes, our new models predict more accurately the background leakage outflows, especially in pipes presenting strong levels of leakages, due, e.g., to high degradation levels of the pipes. Moreover, we believe that the gain of accuracy between the state of the art and the new models is strongly correlated to the deltas of elevations and to the head-losses along the pipes. Indeed, important variations of elevations and head-losses make the pressure-heads along the pipes to vary significantly too, and then should increase the benefit in using our models. In some situations, our new models could even permit to identify partly-unsupplied pipes or high-lying nodes, by detecting zero pressure locations along the pipes.

Despite their complexity, our new models can be easily integrated into existing software programs, providing that their solvers allow to deal with possibly large and ill-conditioned systems. For this purpose, we implemented an efficient Newton algorithm including several numerical enhancements. Deeper explanations of these enhancements are available in the supplementary material. Thereby, our solver permits to simulate large networks in an acceptable time.

The characterization of the level of leakages in WDNs is of prime importance for operators and decision makers. Two of our new models take explicitly into account the pressure-heads at both extremities of each pipe, and thus permit the calibration of both leakage types and degradation levels of pipes. Hence, they pave the way to more reliable decision support tools (e.g., for choosing the pipes which have to be repaired and/or replaced first). Nevertheless, this potential application needs first to evaluate the expected values of the parameters for these new models, from physical measures in several and contrasted real leaky networks.

Finally, all our code is part of the Python collaborative framework OOPNET [27, 28], and will be available on the GitHub public repository[5] of the project soon. This way, we are convinced that our work, which represents a significant step forward from the previous state of knowledge, will be easily profitable to the whole community of WDN modelers.

Declaration of competing interest

The authors declare that they have no known competing financial interests or personal relationships that could have appeared to influence the work reported in this paper.

Funding

---

[5]`https://github.com/oopnet`

References

[1] S. Ateş. Hydraulic modelling of closed pipes in loop equations of water distribution networks. *Applied Mathematical Modelling*, 40(2):966–983, Jan. 2016. ISSN 0307-904X. doi: 10.1016/j.apm.2015.06.017. URL `https://www.sciencedirect.com/science/article/pii/S0307904X15003960`.

[2] L. Berardi, D. Laucelli, R. Ugarelli, and O. Giustolisi. Hydraulic System Modelling: Background Leakage Model Calibration in Oppegård Municipality. In *Procedia Engineering*, volume 119 of *Computing and Control for the Water Industry (CCWI2015) Sharing the best practice in water management*, pages 633–642, Jan. 2015. doi: 10.1016/j.proeng.2015.08.916. URL `http://www.sciencedirect.com/science/article/pii/S1877705815025862`.

[3] P. Boulos and T. Altman. A graph-theoretic approach to explicit nonlinear pipe network optimization. *Applied Mathematical Modelling*, 15(9):459–466, Sept. 1991. ISSN 0307-904X. doi: 10.1016/0307-904X(91)90035-N. URL `https://www.sciencedirect.com/science/article/pii/0307904X9190035N`.

[4] B. Coulbeck. Dynamic simulation of water distribution systems. *Mathematics and Computers in Simulation*, 22(3): 222–230, Sept. 1980. ISSN 0378-4754. doi: 10.1016/0378-4754(80)90049-X. URL `https://www.sciencedirect.com/science/article/pii/037847548090049X`.

[5] E. Creaco and T. Walski. Economic Analysis of Pressure Control for Leakage and Pipe Burst Reduction. *Journal of Water Resources Planning and Management*, 143(12):04017074, Dec. 2017. doi: 10.1061/(ASCE)WR.1943-5452. 0000846. URL `https://ascelibrary.org/doi/full/10.1061/(ASCE)WR.1943-5452.0000846`.

[6] T. A. Davis. *Direct Methods for Sparse Linear Systems*. Fundamentals of Algorithms. Society for Industrial and Applied Mathematics, Jan. 2006. ISBN 978-0-89871-613-9. doi: 10.1137/1.9780898718881. URL `https://epubs.siam.org/doi/book/10.1137/1.9780898718881`.

[7] K. Diao, Z. Wang, G. Burger, C.-H. Chen, W. Rauch, and Y. Zhou. Speedup of water distribution simulation by domain decomposition. *Environmental Modelling & Software*, 52:253–263, Feb. 2014. ISSN 13648152. doi: 10.1016/j.envsoft.2013.09.025. URL `https://linkinghub.elsevier.com/retrieve/pii/S1364815213002247`.

[8] S. Elhay and A. R. Simpson. Dealing with Zero Flows in Solving the Nonlinear Equations for Water Distribution Systems. *J. Hydraul. Eng.*, 137(10):1216–1224, Oct. 2011. ISSN 0733-9429, 1943-7900. doi: 10.1061/(ASCE)HY.1943-7900.0000411. URL `http://ascelibrary.org/doi/10.1061/%28ASCE%29HY.1943-7900.0000411`.

[9] S. Elhay, O. Piller, J. Deuerlein, and A. R. Simpson. A Robust, Rapidly Convergent Method That Solves the Water Distribution Equations for Pressure-Dependent Models. *J. Water Resour. Plann. Manage.*, 142(2):04015047, Feb. 2016. ISSN 0733-9496, 1943-5452. doi: 10.1061/(ASCE)WR.1943-5452.0000578. URL `http://ascelibrary.org/doi/10.1061/%28ASCE%29WR.1943-5452.0000578`.

[10] M. Ferrante, E. Todini, C. Massari, B. Brunone, and S. Meniconi. Equivalent hydraulic resistance to simulate pipes subject to diffuse outflows. *Journal of Hydroinformatics*, 14(1):65–74, Jan. 2012. ISSN 1464-7141. doi: 10.2166/hydro.2011.043. URL `/jh/article/14/1/65/3142/Equivalent-hydraulic-resistance-to-simulate-pipes`.

[11] G. Germanopoulos. A technical note on the inclusion of pressure dependent demand and leakage terms in water supply network models. *Civil Engineering Systems*, 2(3):171–179, Sept. 1985. ISSN 0263-0257. doi: 10.1080/02630258508970401. URL `http://www.tandfonline.com/doi/abs/10.1080/02630258508970401`.

[12] O. Giustolisi, D. Savic, and Z. Kapelan. Pressure-Driven Demand and Leakage Simulation for Water Distribution Networks. *Journal of Hydraulic Engineering*, 134(5):626–635, 2008. doi: 10.1061/(ASCE)0733-9429(2008)134:5(626). URL `https://ascelibrary.org/doi/abs/10.1061/(ASCE)0733-9429(2008)134:5(626)`.

[13] O. Giustolisi, L. Berardi, D. Laucelli, D. Savic, T. Walski, and B. Brunone. Battle of Background Leakage Assessment for Water Networks (BBLAWN) at WDSA Conference 2014. *Procedia Engineering*, 89:4–12, Jan. 2014. ISSN 1877-7058. doi: 10.1016/j.proeng.2014.11.153. URL `http://www.sciencedirect.com/science/article/pii/S1877705814022681`.

[14] L. Gyergyek and S. Presern. Simulation and optimal control of large water distribution systems. *Mathematics and Computers in Simulation*, 24(5):385–392, Oct. 1982. ISSN 0378-4754. doi: 10.1016/0378-4754(82)90027-1. URL `https://www.sciencedirect.com/science/article/pii/0378475482900271`.

[15] E. Jaumouillé, O. Piller, and J. E. Van Zyl. A hydraulic model for water distribution systems incorporating both inertia and leakage. In *Water Management Challenges in Global Change (CCWI2007 and SUWM2007 Conference), Leicester, GBR*, pages 3–5, 2007.

[16] I. E. Karadirek, S. Kara, G. Yilmaz, A. Muhammetoglu, and H. Muhammetoglu. Implementation of Hydraulic Modelling for Water-Loss Reduction Through Pressure Management. *Water Resour Manage*, 26(9):2555–2568, July 2012. ISSN 1573-1650. doi: 10.1007/s11269-012-0032-2. URL https://doi.org/10.1007/s11269-012-0032-2.

[17] A. Lambert. What do we know about pressure-leakage relationships in distribution systems? In *IWA Conference 'System Approach to Leakage Control and Water Distribution Systems Management'*, page 8, 2001.

[18] S. Lao, S. Portela, J. Dequesne, and O. Debuf. National report of SISPEA data. Technical Report Edition of Jan. 2022 from data of 2020, French national observatory of water and sanitation services, 2022. URL https://www.services.eaufrance.fr/docs/synthese/rapports/Rapport_Sispea_2020_VF.pdf.

[19] M. Maskit and A. Ostfeld. Leakage Calibration of Water Distribution Networks. In *Procedia Engineering*, volume 89 of *16th Water Distribution System Analysis Conference, WDSA2014*, pages 664–671, Jan. 2014. doi: 10.1016/j.proeng.2014.11.492. URL https://www.sciencedirect.com/science/article/pii/S1877705814026071.

[20] J. May. Pressure dependent leakage. *World water and environmental engineering*, 17(8):10, 1994.

[21] A. Ostfeld, E. Salomons, L. Ormsbee, J. G. Uber, C. M. Bros, P. Kalungi, R. Burd, B. Zazula-Coetzee, T. Belrain, D. Kang, K. Lansey, H. Shen, E. McBean, Z. Yi Wu, T. Walski, S. Alvisi, M. Franchini, J. P. Johnson, S. R. Ghimire, B. D. Barkdoll, T. Koppel, A. Vassiljev, H. Kim Joong, G. Chung, G. Yoo Do, K. Diao, Y. Zhou, J. Li, Z. Liu, K. Chang, J. Gao, S. Qu, Y. Yuan, T. D. Prasad, D. Laucelli, L. S. Vamvakeridou Lyroudia, Z. Kapelan, D. Savic, L. Berardi, G. Barbaro, O. Giustolisi, M. Asadzadeh, B. A. Tolson, and R. McKillop. Battle of the Water Calibration Networks. *Journal of Water Resources Planning and Management*, 138(5):523–532, Sept. 2012. doi: 10.1061/(ASCE) WR.1943-5452.0000191. URL https://ascelibrary.org/doi/10.1061/%28ASCE%29WR.1943-5452.0000191.

[22] O. Piller. *Modeling the behavior of a network - Hydraulic analysis and a sampling procedure for estimating the parameters.* PhD Thesis in Applied Mathematics, University of Bordeaux, France, 1995. URL http://www.theses.fr/1995BOR10511.

[23] O. Piller. *Water distribution system modeling and optimization.* French habilitation, Ecole doctorale Sciences des métiers de l'ingénieur, ED 432, Paris, France, 2019. URL http://rgdoi.net/10.13140/RG.2.2.23972.53122.

[24] O. Piller, B. Bremond, and M. Poulton. Least Action Principles Appropriate to Pressure Driven Models of Pipe Networks. In *World Water & Environmental Resources Congress 2003*, pages 1–15, Philadelphia, Pennsylvania, United States, June 2003. American Society of Civil Engineers. ISBN 978-0-7844-0685-4. doi: 10.1061/40685(2003) 113. URL http://ascelibrary.org/doi/abs/10.1061/40685%282003%29113.

[25] O. Piller, D. Gilbert, K. Haddane, and S. Sabatié. Porteau: An Object-Oriented programming hydraulic toolkit for water distribution system analysis. In *Eleventh International Conference on Computing and Control for the Water Industry (CCWI 2011)*, volume 1/3, pages p. 27 – p. 32, Exeter, United Kingdom, Sept. 2011. Centre for Water Systems, University of Exeter. URL https://hal.archives-ouvertes.fr/hal-00653763.

[26] R. Puust, Z. Kapelan, D. A. Savic, and T. Koppel. A review of methods for leakage management in pipe networks. *Urban Water Journal*, 7(1):25–45, Feb. 2010. ISSN 1573-062X. doi: 10.1080/15730621003610878. URL https://doi.org/10.1080/15730621003610878.

[27] D. Steffelbauer and D. Fuchs-Hanusch. OOPNET: An object-oriented EPANET in Python. *Procedia Engineering*, 119:710–718, 2015. ISSN 18777058. doi: 10.1016/j.proeng.2015.08.924. URL https://linkinghub.elsevier.com/retrieve/pii/S1877705815025941.

[28] D. Steffelbauer, O. Piller, C. Chambon, and E. Abraham. Towards a novel multi-purpose simulation software of water distribution systems in Python. In *14th International Conference on Hydroinformatics, Water INFLUENCE Water INFormatic soLUtions and opEN problems in the cycle from Clouds to ocEan*, page 4, Bucharest, Romania, July 2022.

[29] D. B. Steffelbauer, J. Deuerlein, D. Gilbert, E. Abraham, and O. Piller. Pressure-Leak Duality for Leak Detection and Localization in Water Distribution Systems. *J. Water Resour. Plann. Manage.*, 148(3):04021106, Mar. 2022. ISSN 0733-9496, 1943-5452. doi: 10.1061/(ASCE)WR.1943-5452.0001515. URL https://ascelibrary.org/doi/10.1061/%28ASCE%29WR.1943-5452.0001515.

[30] W. Tinney and W. Meyer. Solution of large sparse systems by ordered triangular factorization | IEEE Journals & Magazine | IEEE Xplore. *IEEE TACON*, 18(4):333 – 346, 1973. ISSN 0018-9286, 1558-2523. doi: 10.1109/TAC.1973.1100352. URL https://ieeexplore.ieee.org/abstract/document/1100352.

[31] P. Virtanen, R. Gommers, T. E. Oliphant, M. Haberland, T. Reddy, D. Cournapeau, E. Burovski, P. Peterson, W. Weckesser, J. Bright, S. J. van der Walt, M. Brett, J. Wilson, K. J. Millman, N. Mayorov, A. R. J. Nelson, E. Jones, R. Kern, E. Larson, C. J. Carey, I. Polat, Y. Feng, E. W. Moore, J. VanderPlas, D. Laxalde, J. Perktold, R. Cimrman, I. Henriksen, E. A. Quintero, C. R. Harris, A. M. Archibald, A. H. Ribeiro, F. Pedregosa, and P. van Mulbregt. SciPy 1.0: fundamental algorithms for scientific computing in Python. *Nature Methods*, 17(3):261–272, Mar. 2020. ISSN 1548-7105. doi: 10.1038/s41592-019-0686-2. URL `https://www.nature.com/articles/s41592-019-0686-2`. Number: 3 Publisher: Nature Publishing Group.

[32] J. M. Wagner, U. Shamir, and D. H. Marks. Water Distribution Reliability: Simulation Methods. *Journal of Water Resources Planning and Management*, 114(3):276–294, May 1988. ISSN 0733-9496, 1943-5452. doi: 10.1061/(ASCE) 0733-9496(1988)114:3(276). URL `http://ascelibrary.org/doi/10.1061/%28ASCE%290733-9496%281988%29114%3A3%28276%29`.

[33] T. M. Walski, D. V. Chase, D. Savic, W. Grayman, S. Beckwith, E. Koelle, and I. Haestad Methods. *Advanced water distribution modeling and management*. Bentley Institute Press, Exton, PA, 2007. ISBN 978-1-934493-01-4. OCLC: 154213231.

[34] G. S. Williams, A. Hazen, and others. *Hydraulic tables: the elements of gagings and the friction of water flowing in pipes, aqueducts, sewers, etc.* J. Wiley & sons, inc.: London, Chapman & Hall, limited,, 1933.

Numerical enhancements of the Newton algorithm, and calibration of the leakage parameters of a leaky pipe

Supplementary material of the article:

Modeling of pressure-dependent background leakages in water distribution networks

Camille Chambon[a,b,*], Olivier Piller[a,c], Iraj Mortazavi[b]

[a]*INRAE, UR ETTIS, Cestas, F-33612, France*
[b]*CNAM, M2N, Paris, F-75003, France*
[c]*School of Civil, Environmental, and Mining Eng., Adelaide, SA 5005, Australia*

*Corresponding author.
Email address:* `camille.chambon@inrae.fr` (Camille Chambon)

1. Numerical enhancements of the Newton algorithm

In our article, we propose to use a Newton algorithm to compute the flow rates in pipes and the heads at junctions in water distribution networks (WDNs) at equilibrium. To maintain the stability of this algorithm, we integrate several numerical enhancements into it. This section explains and illustrates these enhancements.

1.1. Regularization of the Hazen-Williams friction head loss and of its derivative

At each iteration of the Newton algorithm, we need, to compute the Schur complement of the Jacobian matrix, to inverse the derivative of the friction head-loss along each pipe with respect to the flow rate at the middle of the pipe. For models M0 and Ref, the friction head-loss is computed with the Hazen-Williams formula [s9], as:

$$\xi_\ell(q_{0.5}) = f\,\ell\,q_{0.5}\big|q_{0.5}\big|^{\gamma-1}, \tag{s1}$$

where $\gamma = 1.852$, $f \in \mathbb{R}_*^+$, $\ell \in \mathbb{R}_+^*$ and $q_{0.5} \in \mathbb{R}$ are respectively the Hazen-Williams exponent, the friction coefficient, the length of the pipe and the flow rate at the middle of the pipe. Thus, the derivative of eq. (s1) with respect to $q_{0.5}$ is computed as:

$$\frac{\mathrm{d}\xi_\ell}{\mathrm{d}q_{0.5}}(q_{0.5}) = \gamma\,f\,\ell\,\big|q_{0.5}\big|^{\gamma-1}. \tag{s2}$$

Equation (s2) is 0 when $q_{0.5} = 0$, which leads to a division by zero error when computing its inverse.

To prevent this error, [s6] proposed a cubic regularization of eq. (s1), and a quadratic regularization of eq. (s2), for $q_{0.5}$ close to 0. We decide to reuse these regularizations. We illustrate them on fig. s1 for a pipe of length $\ell = 1\,\mathrm{m}$ and friction coefficient $f = 1\,\mathrm{s}^{1.852}\,\mathrm{l}^{-1.852}$, without any loss of generality. Indeed, eq. (s1), eq. (s2) and their regularizations depend linearly on ℓ and f. Thus, fig. s1 can be transposed to any other ℓ an f, by just multiplying the values plotted on the vertical axis by ℓ and f.

(a) $\xi_\ell(q_{0.5})$

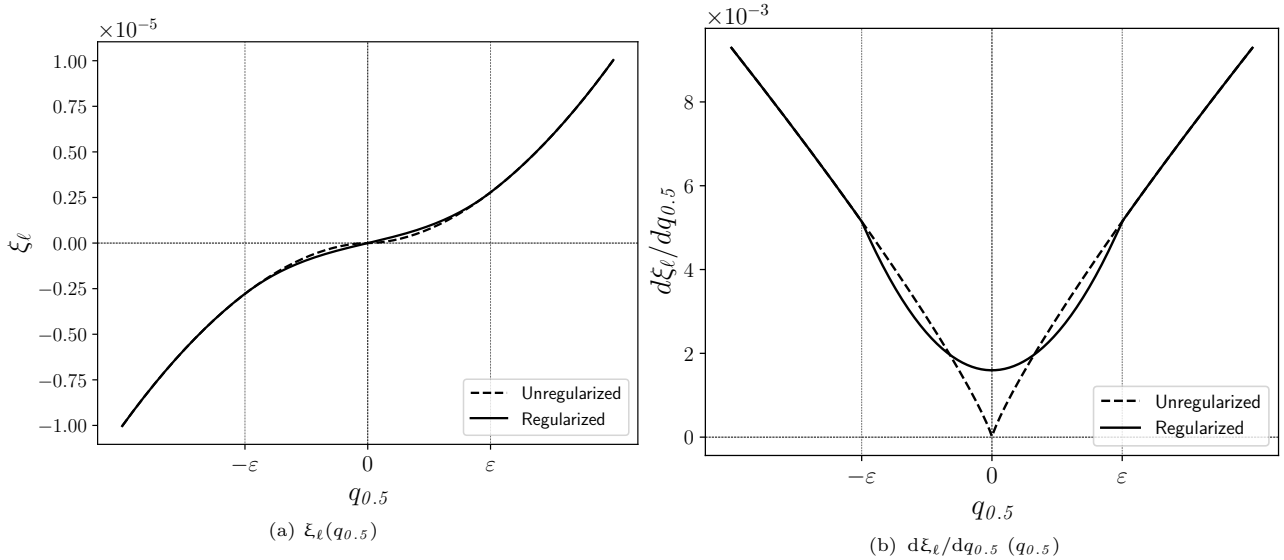(b) $\mathrm{d}\xi_\ell/\mathrm{d}q_{0.5}\,(q_{0.5})$

Figure s1: Cubic regularization of the Hazen-Williams friction head loss function $\xi_\ell(q_{0.5})$ [s9] (in mH$_2$O, fig. s1a), and quadratic regularization of its derivative $\mathrm{d}\xi_\ell/\mathrm{d}q_{0.5}\,(q_{0.5})$ (in mH$_2$O l^{-1} s, fig. s1b), in a pipe of length $\ell = 1\,\mathrm{m}$ and friction coefficient $f = 1\,\mathrm{s}^{1.852}\,\mathrm{l}^{-1.852}$, for flow rates at the middle of the pipe $q_{0.5}$ close to $0\,\mathrm{l\,s^{-1}}$, as initially proposed by [s6]. Here, $\varepsilon = 10^{-3}\,\mathrm{l\,s^{-1}}$, which is also the value of ε used in the source code.

1.2. Regularizations of the Wagner consumption

To compute the Schur complement of the Jacobian matrix, we also need, for each model, to compute at each junction node the derivative of the user consumption with respect to the pressure-head at that node. To compute the user consumption, we choose the Wagner pressure-outflow relationship (POR) [s8], such that

$$c(p) = \begin{cases} 0 & \text{if } p \le p_m \\ d\sqrt{\dfrac{p - p_m}{p_s - p_m}} & \text{if } p_m < p < p_s \\ d & \text{if } p \ge p_s, \end{cases} \tag{s3}$$

2

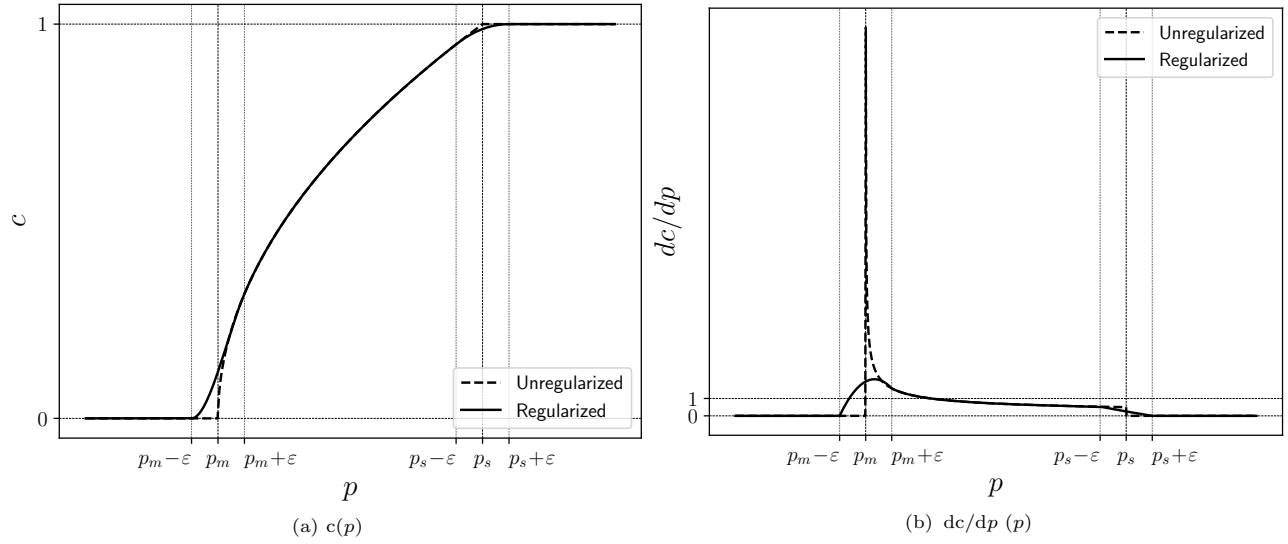(a) c(p) (b) dc/dp (p)

Figure s2: Cubic regularizations of the Wagner user consumption function c(p) [s8] (in $1\,\mathrm{s}^{-1}$, fig. s2a), and quadratic regularizations of its derivative dc/dp (p) (in $1\,\mathrm{s}^{-1}\,\mathrm{mH_2O}^{-1}$, fig. s2b), at a junction node where demand $d = 1\,1\mathrm{s}^{-1}$, and any minimum pressure-head p_m and service pressure-head p_s such that $p_m \geq 0\,\mathrm{mH_2O}$ and $p_s > p_m$, for local pressure-heads p close to p_m and p_s, as initially proposed by [s7]. Here, ε is chosen equal to $0.1\,\mathrm{mH_2O}$ for better readability, but in the source code $\varepsilon = 10^{-3}\,\mathrm{mH_2O}$.

where $p \in \mathbb{R}^+$ and $d \in \mathbb{R}^+$ are respectively the local pressure-head and the user demand at the junction node, and $p_m \in \mathbb{R}^+$ and $p_s \in \mathbb{R}^+_*$ are respectively the minimum and the service pressure-heads, such that $p_m < p_s$. Thus, the derivative of eq. (s3) with respect to p is

$$\frac{\mathrm{dc}}{\mathrm{d}p}(p) = \begin{cases} d\,\dfrac{1}{p_s - p_m}\,\dfrac{1}{2\sqrt{\dfrac{p - p_m}{p_s - p_m}}} = \dfrac{\mathrm{c}(p)}{2\,(p - p_m)} & \text{if } p_m < p < p_s \\ 0 & \text{otherwise.} \end{cases} \tag{s4}$$

Equation (s4) is undefined at $p = p_m$ and discontinuous at $p = p_s$, which could lead to convergence failure when p is close to p_m and p_s.

To make eq. (s4) continuous $\forall p \in \mathbb{R}$, [s7] proposed two cubic regularizations of eq. (s3), and two quadratic regularizations of eq. (s4), when p is close to p_m and p_s. We decide to reuse these regularizations. Figure s2 illustrates them for a junction node where demand $d = 1\,1\mathrm{s}^{-1}$, and any minimum pressure-head p_m and service pressure-head p_s such that $p_m \geq 0\,\mathrm{mH_2O}$ and $p_s > p_m$, without any loss of generality. Indeed, eq. (s3), eq. (s4) and their regularizations depend linearly on d. Thus, fig. s2 can be transposed to any other d, by just multiplying the values plotted on the vertical axis by d.

1.3. Regularization of lineic leakage outflow and of its derivative

At each iteration of the Newton algorithm, we also compute, in each leaky pipe, the lineic leakage outflow for one or several local pressure-head(s), and its derivative with respect to that pressure-head(s). To compute the lineic leakage outflow, we choose the formula of [s3], defined as

$$\mathrm{q_{LL}}(p) = \beta\left([p]^+\right)^\alpha, \tag{s5}$$

where $p \in \mathbb{R}^+$ is a local pressure-head, $[\widetilde{p}]^+$ its positive part, and $\alpha \in\,]0.5, 2.5]$ and $\beta \in \left[10^{-7}, 10^{-1}\right]\,1\mathrm{s}^{-1}\,\mathrm{m}^{-1-\alpha}$ are the leakage parameters. Thus, the derivative of eq. (s5) with respect to p is

$$\frac{\mathrm{dq_{LL}}}{\mathrm{d}p}(p) = \begin{cases} \alpha\,\beta\,p^{\alpha-1} & \text{if } p > 0 \\ 0 & \text{otherwise.} \end{cases} \tag{s6}$$

Equation (s6) is discontinuous at $p = 0$ $\forall \alpha \in\,]0.5, 1[$, which could lead to convergence failure.

To make eq. (s6) continuous $\forall p \in \mathbb{R}$ and $\forall \alpha \in\,]0.5, 2.5[$, we propose a new cubic regularization of eq. (s5) and a new quadratic regularization of eq. (s6) for p close to 0. Figures s3a and s3b illustrate this regularization when $\alpha = 0.6$ and $\beta = 10^{-4}\,1\mathrm{s}^{-1}\,\mathrm{m}^{-1-\alpha}$, without any loss of generality. Indeed, eq. (s5), eq. (s6) and their regularizations depend linearly on β. Thus, figs. s3a and s3b can be transposed to any other β, by just multiplying the values plotted on the vertical axis

(a) $q_{LL}(p)$ for $\alpha = 0.6$.

(b) $dq_{LL}/dp\ (p)$ for $\alpha = 0.6$.

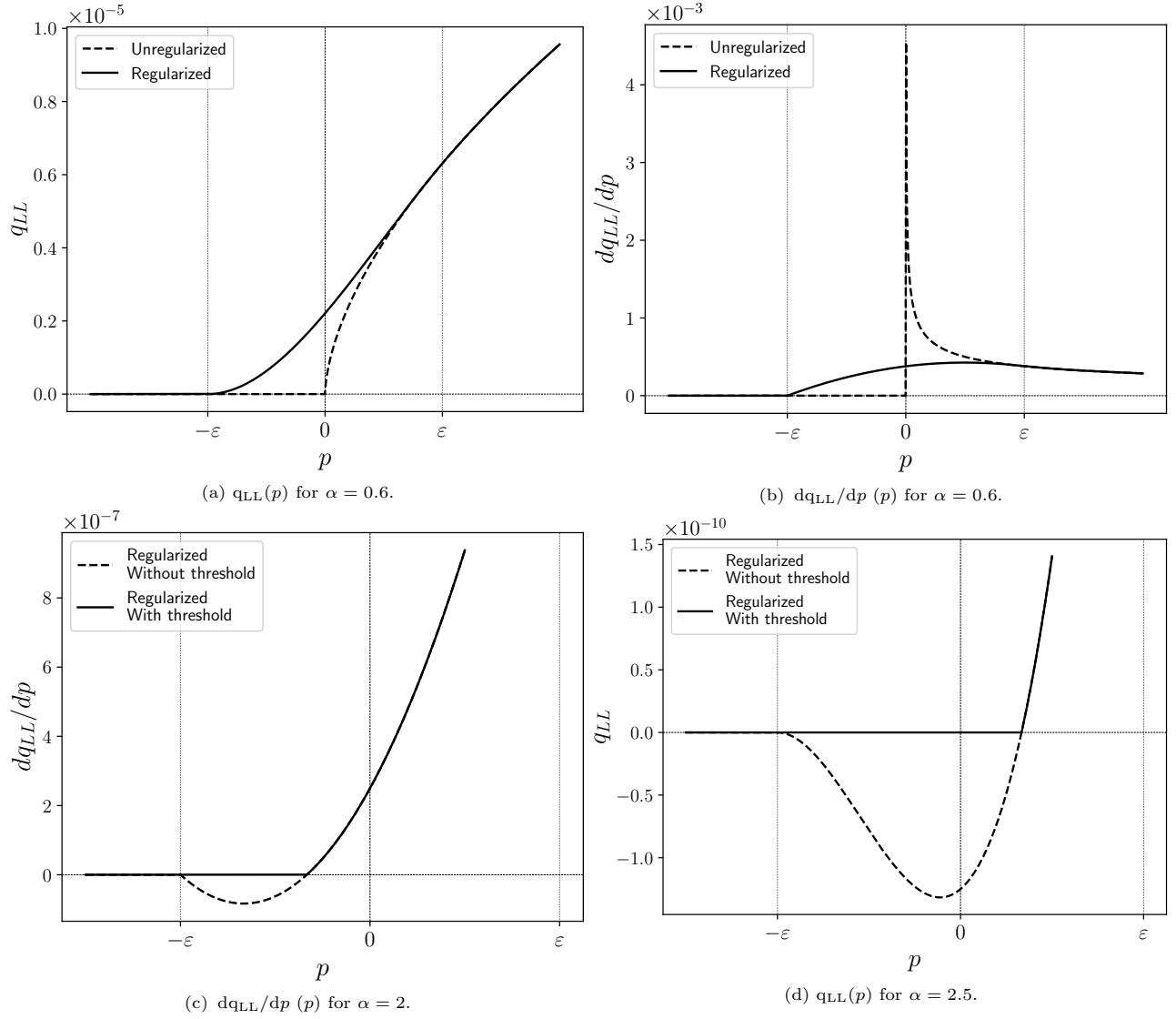(c) $dq_{LL}/dp\ (p)$ for $\alpha = 2$.

(d) $q_{LL}(p)$ for $\alpha = 2.5$.

Figure s3: New cubic regularization of the lineic leakage outflow function $q_{LL}(p)$ [s3] (in $1\,s^{-1}\,m^{-1}$, figs. s3a and s3d) and quadratic regularization of its derivative $dq_{LL}/dp\ (p)$ (in $1\,s^{-1}\,m^{-1}\,mH_2O^{-1}$, figs. s3b and s3c), in a pipe with leakage type $\alpha \in \{0.6, 2, 2.5\}$ (unit-less), degradation level $\beta = 10^{-4}\ 1\,s^{-1}\,m^{-1-\alpha}$, for local pressure-heads p close to $0\,mH_2O$. Here, ε is chosen equal to $10^{-2}\,mH_2O$ for better readability, but in the source code $\varepsilon = 10^{-3}\,mH_2O$.

by $\beta/10^{-4}$. However, our new regularizations can induce negative q_{LL} when $\alpha \geq 2$. In this case, we choose to set q_{LL} to 0. Figures s3c and s3d illustrate this threshold for $\alpha \in \{2, 2.5\}$ and $\beta = 10^{-4}\ 1\,s^{-1}\,m^{-1-\alpha}$.

1.4. Preconditioning of the Jacobian matrix

The magnitude of the elements in the Jacobian matrix may vary strongly from one part of a WDN to another, according to user demands, tank levels, use of pumps and/or valves, etc. Thus, using the Jacobian matrix as it is defined in our article may cause instabilities in the Newton algorithm, and increase significantly the number of iterations needed to converge.

Like [s6], [s1] proposed a method to improve the stability of the Newton's algorithm when some flow rates are close to 0. To do so, denoting n_p the number of pipes in the WDN, [s1] limited, at each Newton iteration m, each singular value $\lambda_k^{(m)}$ of $\boldsymbol{J_{11}^{(m)}}$, $k \in \{1, .., n_p\}$, by a minimum value $\lambda_{min}^{(m)}$ defined as

$$\lambda_{min}^{(m)} = \frac{\lambda_{max}^{(m)}}{\kappa_{max}}, \tag{s7}$$

where $\lambda_{max}^{(m)}$ is such that

$$\lambda_{max}^{(m)} = \max_k \left(\left[\boldsymbol{J_{11}^{(m)}} \right]_{kk} \right), \tag{s8}$$

4

and κ_{max} corresponds to a maximum threshold condition number (e.g., $\kappa_{max} = 10^{10}$). Like so, [s1] did not only avoid null derivatives on the diagonal of $\boldsymbol{J}_{11}^{(m)}$, but also reduced the difference of magnitude order between all diagonal elements of $\boldsymbol{J}_{11}^{(m)}$. However, the preconditioning method proposed by [s1] only applies to the case where consumptions are independent of the pressure and when there is no leakage.

Thus, we choose to extend the method proposed by [s1], to make it now deal with pressure-dependent consumptions and leakages. To do so, we recompute $\lambda_{max}^{(m)}$ taking into account all non-null elements of $\boldsymbol{J}_{11}^{(m)}$, $\boldsymbol{J}_{12}^{(m)}$ and $\boldsymbol{J}_{22}^{(m)}$, such that:

$$\lambda_{max}^{(m)} = \max\left(\max_k\left(\left|\left[\boldsymbol{J}_{11}^{(m)}\right]_{kk}\right|\right), \max_{ki}\left(\left|\left[\boldsymbol{J}_{12}^{(m)}\right]_{ki}\right|\right), \max_{ij}\left(\left|\left[\boldsymbol{J}_{22}^{(m)}\right]_{ij}\right|\right)\right), \tag{s9}$$
$$\{i,j,k\} \in \{1,..,n_j\} \times \{1,..,n_j\} \times \{1,..,n_p\}$$

and we recompute $\lambda_{min}^{(m)} = \lambda_{max}^{(m)}/\kappa_{max}$. Finally, we limit:
- each element on the diagonal of $\boldsymbol{J}_{11}^{(m)}$ as:

$$\left[\boldsymbol{J}_{11}^{(m)}\right]_{kk} = \max\left(\left|\left[\boldsymbol{J}_{11}^{(m)}\right]_{kk}\right|, \lambda_{min}^{(m)}\right) \times \text{sgn}\left(\left[\boldsymbol{J}_{11}^{(m)}\right]_{kk}\right), \tag{s10}$$

- each non-null element of $\boldsymbol{J}_{12}^{(m)}$ as:

$$\left[\boldsymbol{J}_{12}^{(m)}\right]_{ki} = \max\left(\left|\left[\boldsymbol{J}_{12}^{(m)}\right]_{ki}\right|, \lambda_{min}^{(m)}\right) \times \text{sgn}\left(\left[\boldsymbol{J}_{12}^{(m)}\right]_{ki}\right), \tag{s11}$$

- and each diagonal or non-null element of $\boldsymbol{J}_{22}^{(m)}$ as:

$$\left[\boldsymbol{J}_{22}^{(m)}\right]_{ij} = \max\left(\left|\left[\boldsymbol{J}_{22}^{(m)}\right]_{ij}\right|, \lambda_{min}^{(m)}\right) \times \text{sgn}\left(\left[\boldsymbol{J}_{22}^{(m)}\right]_{ij}\right), \tag{s12}$$

where sgn(.) represents the sign function, and is used to conserve the sign of the regularized elements.

1.5. Damping scheme with Goldstein's line search on weighted least squares

To reduce the number of iterations needed by the Newton algorithm to reach convergence, [s2] proposed a damping method based on a line search approach. To summary, this strategy first looks for the descent directions along which the residuals will be reduced, and then computes a step size that determines how far the iterates can move along that direction. We decide to reuse this damping method in our models, extending it to integrate pressure-dependent background leakages too.

In their damping method, [s2] first denoted the diagonal matrix of positive weights $\boldsymbol{W} \in \mathbb{R}^{(n_p+n_j)\times(n_p+n_j)}$, where n_p and n_j are respectively the number of pipes and junction nodes in the WDN. Next, [s2] denoted the weighted least squares (WLS) objective scalar function

$$\theta(\boldsymbol{q_{0.5}}, \boldsymbol{h}) = \frac{1}{2}\left\|\boldsymbol{W}^{\frac{1}{2}}\boldsymbol{\rho}(\boldsymbol{q_{0.5}}, \boldsymbol{h})\right\|_2^2 = \frac{1}{2}\boldsymbol{\rho}^T\boldsymbol{W}\boldsymbol{\rho}, \tag{s13}$$

where $\boldsymbol{q_{0.5}}$ and $\boldsymbol{h}$ are respectively the flows at the middles of pipes and the heads at junctions, and $\boldsymbol{\rho}$ are the residuals (including both mass and energy residuals) such that $\boldsymbol{\rho} = \boldsymbol{\rho}(\boldsymbol{q_{0.5}}, \boldsymbol{h})$. Next, from eq. (s13), [s2] defined the optimization problem to solve as:

$$\min_{\boldsymbol{q_{0.5}}, \boldsymbol{h}} \theta(\boldsymbol{q_{0.5}}, \boldsymbol{h}), \tag{s14}$$

and the damped scheme to solve eq. (s14) consists in computing:

$$\begin{pmatrix} \boldsymbol{q_{0.5}}^{(m+1)} \\ \boldsymbol{h}^{(m+1)} \end{pmatrix} = \begin{pmatrix} \boldsymbol{q_{0.5}}^{(m)} \\ \boldsymbol{h}^{(m)} \end{pmatrix} + \sigma^{(m)}\begin{pmatrix} \boldsymbol{\delta_{q_{0.5}}}^{(m)} \\ \boldsymbol{\delta_h}^{(m)} \end{pmatrix} \tag{s15}$$

with $\sigma^{(m)}$ a step-size. To select the correct $\sigma^{(m)}$, [s2] used the Goldstein criteria scalar function [s5]:

$$g(\theta^{(m)}, \sigma^{(m)}) = \frac{\theta^{(m)} - \theta(\hat{\boldsymbol{q}}_{0.5}^{(m+1)}, \hat{\boldsymbol{h}}^{(m+1)})}{2\,\sigma^{(m)}\theta^{(m)}}, \tag{s16}$$

where

$$\begin{pmatrix} \hat{\boldsymbol{q}}_{0.5}^{(m+1)} \\ \hat{\boldsymbol{h}}^{(m+1)} \end{pmatrix} = \begin{pmatrix} \boldsymbol{q_{0.5}}^{(m)} \\ \boldsymbol{h}^{(m)} \end{pmatrix} + \sigma^{(m)}\begin{pmatrix} \boldsymbol{\delta_{q_{0.5}}}^{(m)} \\ \boldsymbol{\delta_h}^{(m)} \end{pmatrix}, \tag{s17}$$

in an algorithm which divides $\sigma^{(m)}$ by 2 until $g(\theta^{(m)}, \sigma^{(m)}) \geq 0.1$ (unit-less).

To compute the weights $\boldsymbol{W}$, [s2] used the demands at junctions $\boldsymbol{d}$ and the heads at fixed-head nodes $\boldsymbol{h_f}$. To extend their damping method to pressure-dependent background leakages, we now also use the leakage outflows $\boldsymbol{q_L}$ (in $1s^{-1}$) reported to junctions, defined at any junction $j \in \{1..n_j\}$ as

$$q_{L,j} = \sum_{k \in \mathbb{P}_j^-} \int_{\ell_k/2}^{\ell_k} q_{\mathrm{LL}k}(x_k)\, \mathrm{d}x_k + \sum_{k \in \mathbb{P}_j^+} \int_0^{\ell_k/2} q_{\mathrm{LL}k}(x_k)\, \mathrm{d}x_k, \tag{s18}$$

where $\mathbb{P}_j^-$ and $\mathbb{P}_j^+$ are the sets of pipes respectively entering and leaving the node j, ℓ_k is the length of pipe $k \in \mathbb{P}_j^- \cup \mathbb{P}_j^+$, and $q_{\mathrm{LL}k}(x_k)$ is the lineic leakage outflow at the position x_k of k. Then, we compute the weights $\boldsymbol{W}$ as

$$\boldsymbol{W} = \begin{pmatrix} \boldsymbol{M}^{-1} & \boldsymbol{0} \\ \boldsymbol{0} & \boldsymbol{N}^{-1} \end{pmatrix}, \tag{s19}$$

with

$$\boldsymbol{M} = \left(\max_{i \in \{1,..,n_f\}} \boldsymbol{h_{f,i}} \right)^2 \boldsymbol{I_{n_p}} \qquad \text{and} \qquad \boldsymbol{N} = \left(\max_{j \in \{1,..,n_j\}} (\boldsymbol{d_j} + \boldsymbol{q_{L,j}}) \right)^2 \boldsymbol{I_{n_j}}, \tag{s20}$$

where $\boldsymbol{I_{n_p}}$ and $\boldsymbol{I_{n_j}}$ are the $n_p \times n_p$ and $n_j \times n_j$ identity matrices.

2. Calibration of background leakage parameters

In our article, we propose several background leakage models, denoted $\{M0, M1, M2, M3\}$. Model M0 corresponds to the state of the art one, as initially proposed by [s4]. Models $\{M1, M2, M3\}$ are new gradually refined versions of M0.

In this section, we propose a method to calibrate the leakage parameters $\{\alpha, \beta\}$ for each model, considering a single leaky pipe of length ℓ, and supposing that all needed measured data are available.

2.1. State of the art background leakage model (M0)

To calibrate the leakage parameter β associated to model M0, denoted hereafter β^{M0}, we suppose that the pressure-heads at pipe extremities and the flow rate at pipe end have been measured, and we denote them respectively p_0^{meas}, p_ℓ^{meas} and q_ℓ^{meas}. Then, denoting u_0 and u_ℓ the elevations (in m) at the start and end of the pipe, and knowing that, at any $x \in [0, \ell]$, the pressure-head p_x, the elevation u_x and the head h_x are linked by the relation

$$h_x = p_x + u_x, \tag{s21}$$

we also have the particular relations

$$h_0^{meas} = p_0^{meas} + u_0 \qquad \text{and} \qquad h_\ell^{meas} = p_\ell^{meas} + u_\ell. \tag{s22}$$

Next, we suppose that the sources of head-loss other than the friction one are negligible. Thus, we can compute, from h_0^{meas} and h_ℓ^{meas}, the total head-loss along the full pipe as

$$\xi_\ell^{meas} = h_\ell^{meas} - h_0^{meas}, \tag{s23}$$

and the flow at the middle of the pipe, $q_{0.5}^{M0}$, by solving the equation of conservation of energy

$$\xi_\ell^{meas} - f\, \ell\, q_{0.5}^{M0} \left| q_{0.5}^{M0} \right|^{\gamma-1} = 0. \tag{s24}$$

Next, denoting $q_{LL}^{M0} = q_{\mathrm{LL}}^{M0}(x)$, the equation of conservation of the mass at $x = \ell$ is defined as:

$$q_{0.5}^{M0} - \frac{\ell}{2} q_{LL}^{M0} - q_\ell^{meas} = 0, \tag{s25}$$

and thus permits to calculate q_{LL}^{M0} as:

$$q_{LL}^{M0} = \frac{2 \left(q_{0.5}^{M0} - q_\ell^{meas} \right)}{\ell}. \tag{s26}$$

Finally, defining, from $p_0^{meas} = h_0^{meas} - u_0$ and $p_\ell^{meas} = h_\ell^{meas} - u_\ell$, the mean measured pressure-head in the pipe as

$$\widetilde{p^{meas}} = \left(p_0^{meas} + p_\ell^{meas} \right) / 2, \tag{s27}$$

and supposing that $\widetilde{p^{meas}} > 0$, we obtain, $\forall \alpha \in \,]0.5, 2.5]$:

$$\beta^{\text{M0}} = \frac{q_{LL}^{\text{M0}}}{\left(\widetilde{p^{meas}}\right)^{\alpha}}. \tag{s28}$$

Notes:
- We choose here to use q_ℓ^{meas} to calibrate β; but using q_0^{meas} in place of q_ℓ^{meas} would give the same calibrated β^{M0}, because $\text{q}^{\text{M0}}(x)$ is symmetrical about $x = \ell/2$.
- It is not possible to calibrate the parameter α because q_{LL}^{M0} is invariant along the pipe.

2.2. Lineic leakage outflow invariant along the pipe but affine flow rate (M1)

To calibrate the leakage parameter β, we suppose, as for model M0, that the pressure-heads at pipe extremities and the flow rate at pipe end have been measured, and we denote them p_0^{meas}, p_ℓ^{meas} and q_ℓ^{meas}. Thus, we also have $\xi_\ell^{meas} = p_\ell^{meas} + u_\ell - p_0^{meas} - u_0$, and we can compute q_{LL}^{M1} by solving the equation of conservation of energy along the full pipe:

$$\xi_\ell^{meas} - \frac{f}{(\gamma+1)\, q_{LL}^{\text{M1}}} \left(\left|\text{q}_0^{\text{M1}}(q_{LL}^{\text{M1}})\right|^{(\gamma+1)} - \left|q_\ell^{meas}\right|^{(\gamma+1)}\right) = 0, \tag{s29}$$

where

$$\text{q}_0^{\text{M1}}(q_{LL}^{\text{M1}}) = q_\ell^{meas} + \ell\, q_{LL}^{\text{M1}}. \tag{s30}$$

Finally, as for model M0, we obtain, $\forall \alpha \in \,]0.5, 2.5]$:

$$\beta^{\text{M1}} = \frac{q_{LL}^{\text{M1}}}{\left(\widetilde{p^{meas}}\right)^{\alpha}}, \tag{s31}$$

where $\widetilde{p^{meas}}$ is defined by eq. (s27).
Note: As for model M0, it is not possible to calibrate the parameter α, because q_{LL}^{M1} is invariant along the pipe.

2.3. Affine lineic leakage outflow (M2)

For model M2, we suppose that the pressure-heads and the flow rates at both extremities of the pipe have been measured, and we denote them p_0^{meas}, p_ℓ^{meas}, q_0^{meas} and q_ℓ^{meas}. Then, to calibrate parameters α and β, we first reformulate the functions $\text{q}_{LL}(p)$, $\text{q}^{\text{M2}}(x)$, $\varphi^{\text{M2}}(x)$ and $\xi^{\text{M2}}(x)$ (defined in the article), as functions of $\{\alpha, \beta\}$, such that:

$$\text{q}_{\text{LL0}}(\alpha, \beta) = \beta\left([p_0^{meas}]^+\right)^{\alpha} \quad \text{and} \quad \text{q}_{\text{LL}\ell}(\alpha, \beta) = \beta\left([p_\ell^{meas}]^+\right)^{\alpha}, \tag{s32}$$

$$\text{q}_{0.5}^{\text{M2}}(\alpha, \beta) = q_\ell^{meas} + \frac{\ell}{8}\left(\text{q}_{\text{LL0}}(\alpha, \beta) + 3\,\text{q}_{\text{LL}\ell}(\alpha, \beta)\right), \tag{s33}$$

$$\text{q}_0^{\text{M2}}(\alpha, \beta) = \text{q}_{0.5}^{\text{M2}}(\alpha, \beta) + \frac{\ell}{8}\left(3\,\text{q}_{\text{LL0}}(\alpha, \beta) + \text{q}_{\text{LL}\ell}(\alpha, \beta)\right), \tag{s34}$$

$$\varphi_{0.5}^{\text{M2}}(\alpha, \beta) = f\text{q}_{0.5}^{\text{M2}}(\alpha, \beta)\left|\text{q}_{0.5}^{\text{M2}}(\alpha, \beta)\right|^{\gamma-1}, \tag{s35}$$

and

$$\xi^{\text{M2}}(\alpha, \beta) = f\frac{\ell}{6}\left(\varphi_0^{meas} + \varphi_{0.5}^{\text{M2}}(\alpha, \beta) + \varphi_\ell^{meas}\right), \tag{s36}$$

where $\varphi_0^{meas} = fq_0^{meas}\left|q_0^{meas}\right|^{\gamma-1}$ and $\varphi_\ell^{meas} = fq_\ell^{meas}\left|q_\ell^{meas}\right|^{\gamma-1}$. Then, we compute the calibrated parameters $\{\alpha^{\text{M2}}, \beta^{\text{M2}}\}$ by solving the system

$$\begin{cases} \xi_\ell^{meas} - \xi^{\text{M2}}(\alpha^{\text{M2}}, \beta^{\text{M2}}) = 0 & \text{(s37a)} \\ q_0^{meas} - \text{q}_0^{\text{M2}}(\alpha^{\text{M2}}, \beta^{\text{M2}}) = 0 & \text{(s37b)} \end{cases}$$

where eq. (s37a) and eq. (s37b) are respectively the equations of conservation of energy along the full pipe and of mass at $x = 0$.

2.4. Pseudo-quadratic lineic leakage outflow (M3)

For model M3, we suppose, as for model M2, that the pressure-heads and the flow rates at both extremities of the pipe have been measured, and we denote them p_0^{meas}, p_ℓ^{meas}, q_0^{meas} and q_ℓ^{meas}. Then, to calibrate parameters α and β,

we reuse the functions $q_{LL0}(\alpha, \beta)$ and $q_{LL\ell}(\alpha, \beta)$ defined by eq. (s32), and we reformulate the functions $q_{LL}(\tilde{p})$, $q^{M3}(x)$, $\varphi^{M3}(x)$ and $\xi^{M3}(x)$ (defined in the article), as functions of $\{\alpha, \beta\}$, such that:

$$q_{LL0.5}(\alpha, \beta) = q_{LL}\left(\widetilde{p^{meas}}\right) = \beta\left(\left[\frac{p_0^{meas} + p_\ell^{meas}}{2}\right]^+\right)^\alpha, \tag{s38}$$

$$q_{0.5}^{M3}(\alpha, \beta) = q_\ell^{meas} + \frac{\ell}{24}\left(-q_{LL0}(\alpha, \beta) + 8\,q_{LL0.5}(\alpha, \beta) + 5\,q_{LL\ell}(\alpha, \beta)\right), \tag{s39}$$

$$q_0^{M3}(\alpha, \beta) = q_{0.5}^{M3}(\alpha, \beta) + \frac{\ell}{24}\left(5\,q_{LL0}(\alpha, \beta) + 8\,q_{LL0.5}(\alpha, \beta) - q_{LL\ell}(\alpha, \beta)\right), \tag{s40}$$

$$\varphi_{0.5}^{M3}(\alpha, \beta) = f q_{0.5}^{M3}(\alpha, \beta)\left|q_{0.5}^{M3}(\alpha, \beta)\right|^{\gamma-1}, \tag{s41}$$

and

$$\xi^{M3}(\alpha, \beta) = f\frac{\ell}{6}\left(\varphi_0^{meas} + \varphi_{0.5}(\alpha, \beta) + \varphi_\ell^{meas}\right). \tag{s42}$$

Finally, we can compute the calibrated parameters $\{\alpha^{M3}, \beta^{M3}\}$ by solving the system

$$\begin{cases} \xi_\ell^{meas} - \xi^{M3}(\alpha^{M3}, \beta^{M3}) = 0 & \text{(s43a)} \\ q_0^{meas} - q_0^{M3}(\alpha^{M3}, \beta^{M3}) = 0 & \text{(s43b)} \end{cases}$$

where eq. (s43a) and eq. (s43b) are respectively the equations of conservation of energy along the pipe and of mass at $x = 0$.

Note: writing $q_{LL0.5}(\alpha, \beta) = q_{LL}\left(\widetilde{p^{meas}}\right)$ in eq. (s38), we then suppose that $p_{0.5}^{meas} = \widetilde{p^{meas}}$. Making this assumption is the only way to calibrate the leakage parameters for model M3 if $p_{0.5}^{meas}$ has not been measured.

References

[s1] S. Elhay and A. R. Simpson. Dealing with Zero Flows in Solving the Nonlinear Equations for Water Distribution Systems. *J. Hydraul. Eng.*, 137(10):1216–1224, Oct. 2011. ISSN 0733-9429, 1943-7900. doi: 10.1061/(ASCE)HY.1943-7900.0000411. URL `http://ascelibrary.org/doi/10.1061/%28ASCE%29HY.1943-7900.0000411`.

[s2] S. Elhay, O. Piller, J. Deuerlein, and A. R. Simpson. A Robust, Rapidly Convergent Method That Solves the Water Distribution Equations for Pressure-Dependent Models. *J. Water Resour. Plann. Manage.*, 142(2):04015047, Feb. 2016. ISSN 0733-9496, 1943-5452. doi: 10.1061/(ASCE)WR.1943-5452.0000578. URL `http://ascelibrary.org/doi/10.1061/%28ASCE%29WR.1943-5452.0000578`.

[s3] G. Germanopoulos. A technical note on the inclusion of pressure dependent demand and leakage terms in water supply network models. *Civil Engineering Systems*, 2(3):171–179, Sept. 1985. ISSN 0263-0257. doi: 10.1080/02630258508970401. URL `http://www.tandfonline.com/doi/abs/10.1080/02630258508970401`.

[s4] O. Giustolisi, D. Savic, and Z. Kapelan. Pressure-Driven Demand and Leakage Simulation for Water Distribution Networks. *Journal of Hydraulic Engineering*, 134(5):626–635, 2008. doi: 10.1061/(ASCE)0733-9429(2008)134:5(626). URL `https://ascelibrary.org/doi/abs/10.1061/(ASCE)0733-9429(2008)134:5(626)`.

[s5] A. A. Goldstein. *Constructive real analysis.* Courier Corporation, 2013.

[s6] O. Piller. *Modeling the behavior of a network - Hydraulic analysis and a sampling procedure for estimating the parameters.* PhD Thesis in Applied Mathematics, University of Bordeaux, France, 1995. URL `http://www.theses.fr/1995BOR10511`.

[s7] O. Piller, B. Bremond, and M. Poulton. Least Action Principles Appropriate to Pressure Driven Models of Pipe Networks. In *World Water & Environmental Resources Congress 2003*, pages 1–15, Philadelphia, Pennsylvania, United States, June 2003. American Society of Civil Engineers. ISBN 978-0-7844-0685-4. doi: 10.1061/40685(2003)113. URL `http://ascelibrary.org/doi/abs/10.1061/40685%282003%29113`.

[s8] J. M. Wagner, U. Shamir, and D. H. Marks. Water Distribution Reliability: Simulation Methods. *Journal of Water Resources Planning and Management*, 114(3):276–294, May 1988. ISSN 0733-9496, 1943-5452. doi: 10.1061/(ASCE)0733-9496(1988)114:3(276). URL `http://ascelibrary.org/doi/10.1061/%28ASCE%290733-9496%281988%29114%3A3%28276%29`.

[s9] G. S. Williams, A. Hazen, and others. *Hydraulic tables: the elements of gagings and the friction of water flowing in pipes, aqueducts, sewers, etc.* J. Wiley & sons, inc.: London, Chapman & Hall, limited,, 1933.